**Title**
Exploring the Reactivity of Carbene Cycloadditions with Electronic Structure Theory Calculations and Molecular Dynamics Simulations



**Author**
Sader, Charles Avery

**Publication Date**
2015

Peer reviewed|Thesis/dissertation

UNIVERISTY OF CALIFORNIA

Los Angeles

# Exploring the Reactivity of Carbene Cycloadditions with Electronic Structure Theory Calculations and Molecular Dynamics Simulations

A dissertation submitted in partial satisfaction of the requirements for the degree Doctor of Philosophy in Chemistry

by

Charles Avery Sader

2015

ABSTRACT OF THE DISSERTATION

Exploring the Reactivity of Carbene Cycloadditions
with Electronic Structure Theory Calculations
and Molecular Dynamics Simulations

by

Charles Avery Sader

Doctor of Philosophy in Chemistry
University of California, Los Angeles, 2015
Professor Kendall N. Houk, Chair

The transition structures for the (2+1) cycloadditions of dichlorocarbene, chlorofluorocarbene, and difluorocarbene to cyclohexene, 1–hexene, ethylene, and α–chloroacrylonitrile were located using quantum mechanical methods. In addition, transition structures for the (2+1) cycloadditions of chloromethoxycarbene, fluoromethoxycarbene, and dimethoxycarbene to ethylene and α–chloroacrylonitrile were computed. Except for the reactions with ethylene, these cycloadditions were studied experimentally and computationally by Moss and Krogh–Jespersen (Zhang, M.; Moss, R. A.; Thompson, J.; Krogh–Jespersen, K. *J. Org. Chem.* 2012, *77*, 843–850). As a complement to the work of those groups, we have utilized the distortion/interaction model to understand reactivities and selectivities. Computational methods overestimate the entropies of activation for these carbene cycloadditions. Enthalpies, entropies, and free energies of activation for these carbene cycloadditions were computed with a variety of density functionals and *ab*

*initio* methods relative to carbene-alkene precursor complexes, carbene pyridine ylides, and carbene diazirine ylides. These complexes and ylides are predicted to be unstable in terms of free energy and hence are not a viable explanation for the observed discrepancy between experimental and computed activation parameters. Quantum mechanical/molecular mechanical molecular dynamics simulations were used to determine the timescales of reaction for $CCl_2/CF_2$ + ethylene in the gas phase and in explicit pentane solvent. The course of the reactive event is on the order of tens of femtoseconds, which takes place in a frozen solvent configuration. There is no statistically significant difference between timing of bond gap formation or vibrational energy redistribution between carbene cycloadditions in the condensed phase versus the gas phase.

The dissertation of Charles Avery Sader is approved.

William M. Gelbart

Jane P. Chang

Kendall N. Houk, Committee Chair

University of California, Los Angeles

2015

# DEDICATION

None of this would have been possible without the incredible gifts and faithfulness of the Lord God Almighty. I would like to dedicate this dissertation to my wife, Christine, and our two children, Everett Brice and Amelia Mabel. Their support and patience with me throughout this process has been nothing short of supernatural and my pursuit of a graduate degree has been as much for them as it has been for myself.

TABLE OF CONTENTS

# ACKNOWLEDGMENTS

I am grateful to the National Institutes of Health for financial support (R01 GM036700). Many colleagues, too many to name, have provided helpful discussions and suggestions for the work presented in this dissertation. I am especially grateful for the hands-on training with VENUS/NWChem provided by Professor Bill Hase and Swapnil Kohale at Texas Tech University. Also, Professor Chuck Doubleday consulted numerous times on the practical details of running molecular dynamics simulations. Our very own molecular dynamics subgroup in the Houk group was another large database of instruction and critique, especially Professor Peng Liu, Zhongyue Yang, and Jiyong Park. I am thankful to all of the Houk group, and to Ken himself. He is truly a great scientist with innumerable fantastic ideas and a kind man. It was an honor to work with him.

Charles Avery Sader
3245 S Sepulveda Blvd, Apt 102
Los Angeles, CA 90034
(858) 334-9495
avery@chem.ucla.edu

## Education

**B.S. with Honors in Biochemistry**, 2008
*University of Texas at Arlington*, Arlington, Texas

## Experience

***University of California, Los Angeles**, 2009–present*
**Graduate Student Researcher**, PI: Kendall N. Houk

- Performed QM/MM molecular dynamics simulations with VENUS/NWChem and AMBER on carbene cycloadditions in explicit solvent
- Quantified barriers of carbene cycloadditions in terms of computed distortion and interaction energies
- Employed QM calculations with Gaussian09 to assess the energies of various carbene rearrangement pathways
- Computationally explored electrocyclic ring openings of strained cyclobutenes
- Composed scripts with Python and Bash to accelerate data analysis

***University of California, Los Angeles**, 2009–2011*
**Teaching Assistant**

- Organized discussions for undergraduate general and organic chemistry
- Developed quiz and exam questions

## Publications

(1) Sader, C. A.; Houk, K. N. "Distortion/Interaction Analysis of the Reactivities and Selectivities of Halo– and Methoxy–Substituted Carbenes with Alkenes." *ARKIVOC* **2014** (*iii*), 170–183.

(2) Sader, C. A.; Houk, K. N. "A Theoretical Study of Cyclohexyne Addition to Carbonyl–$C_\alpha$ Bonds: Allowed and Forbidden Electrocyclic and Nonpericyclic Ring–Openings of Strained Cyclobutenes." *J. Org. Chem.* **2012**, *77*, 4939–4948.

## Presentations

(1) Sader, C. A.; Houk, K. N. "A Theoretical Study of Cyclohexyne Addition to Carbonyl–$C_\alpha$ Bonds: Allowed and Forbidden Electrocyclic and Nonpericyclic Ring–Openings of Strained Cyclobutenes." 243$^{rd}$ National Meeting of the American Chemical Society, San Diego, CA, March 28, 2012. (Poster presentation)

# I. Distortion/Interaction Analysis of the Reactivities and Selectivities of Halo– and Methoxy–substituted Carbenes with Alkenes

## Introduction

The cycloadditions of carbenes to alkenes constitute a general method for synthesis of cyclopropane ring structures. These cycloadditions have excited widespread interest in the mechanistic details of this reaction. Hoffmann predicted that a $C_{2v}$ cyclic four–electron transition state in which both C–C bonds form simultaneously is orbital–symmetry forbidden;[1,2] therefore, non–least motion approach was proposed by Hoffmann[2] and Moore[3] in which there is initial interaction of the electrophilic empty *p*–orbital (LUMO) of the carbene with the nucleophilic filled π–orbital (HOMO) of the alkene.[1] This prediction was subsequently verified many times with semiempirical[4–6] and ab initio methods[7,8] and was shown to be influenced by a second pair of orbital interactions between the lone pair (HOMO) of the carbene with the π* antibonding orbital (LUMO) of the alkene, which becomes dominant for electron-donor substituted carbenes.[8]

Carbene cycloadditions have been extensively studied experimentally and computationally by the groups of Moss and Krogh–Jespersen over the last decade.[9–12] They combined laser flash photolysis and density functional theory calculations to determine activation parameters for a series of carbene cycloadditions.[13] They found that trends in $\Delta E^{\ddagger}$ parallel expectations based on considerations of carbene stability and nucleophilicity. As a complement to the work of those groups, we have computationally investigated the (2+1) cycloadditions of dihalocarbenes **1a-c** to cyclohexene (**2a**) and 1-hexene (**2b**), as well as the cycloadditions of **1a-c** and methoxycarbenes **1d-f** to ethylene (**2c**) and α–chloroacrylonitrile (**2d**) in the context of the distortion/interaction model of reactivity developed by our group[14] (or the activation–strain model developed independently by Bickelhaupt).[15]

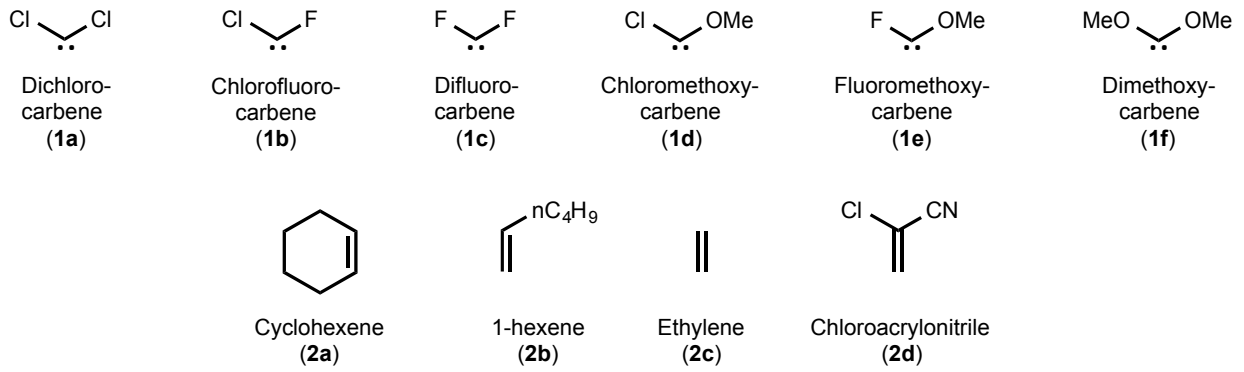


**Figure 1.1.** The carbenes and alkenes employed in this computational study. All except **2c** have been studied experimentally and computationally by Moss and Krogh–Jespersen.[13]

## Computational Methodology

Gas phase reactant, product, and transition state geometry optimizations as well as analytical frequencies were computed using the hybrid meta–GGA functional M06–2X[16] with the 6–31+G(d,p) basis set in the Gaussian 09 suite of programs.[17] Tight convergence criteria and an ultrafine integration grid were used in all optimizations. All reactants have positive definite Hessian matrices and all transition structures have only one negative eigenvalue in their diagonalized force constant matrices. Intrinsic reaction coordinate (IRC)[18,19] calculations were performed to obtain a potential energy surface for distortion/interaction analysis and to ensure that all optimized transition structures connect the appropriate reactants and products.

## Results and Discussion

The distortion/interaction model developed by our group has recently been applied to explain the reactivities and selectivities of (3+2) cycloadditions.[14] This model dissects activation barriers ($\Delta E^{\ddagger}$) of bimolecular reactions into distortion energies ($\Delta E_d^{\ddagger}$) and interaction energies ($\Delta E_i^{\ddagger}$). The distortion energy is the amount of energy required to distort the carbenes and alkenes into their transition state geometries without allowing the cycloaddition partners to interact. The

interaction energy arises from a combination of closed–shell repulsion, charge transfer involving occupied and vacant orbital interactions, electrostatic interactions, and polarization effects. By definition, $\Delta E^{\ddagger} = \Delta E_d^{\ddagger} + \Delta E_i^{\ddagger}$, and the position of the transition state occurs at the point along the reaction coordinate, ζ, where the derivatives of the distortion and interaction energies are equal and opposite ($\delta\Delta E_d(\zeta)/\delta\zeta = -\delta\Delta E_i(\zeta)/\delta\zeta$). Figure 1.2 shows the transition structures for the cycloadditions of **1a–c** with **2a** and **2b** and **1a–f** with **2c** and **2d** computed with M06–2X/6–31+G(d,p). Table 1.1 shows the activation and total distortion energies, the contributions to the distortion energies of the carbene and the alkene, and the interaction energies for reactions of **1a–c** with **2a** and **2b** and **1a–f** with **2c** and **2d**.

**Cycloadditions to cyclohexene and 1–hexene**

As shown in Table 1.1, the cycloadditions of $CCl_2$ (**1a**) and CClF (**1b**) to cyclohexene (**2a**) and 1–hexene (**2b**) have negative activation energies, which are controlled by $\Delta E_i^{\ddagger}$. We found that favorable interaction energy contributes to negative $\Delta E$ at intermediate separation of the carbenes and alkenes studied here and suggests the formation of carbene–alkene precursor complexes, although the existence of these has been debated in the literature.[20–29] We have confirmed π–complexes for cycloadditions to **2a**, **2b**, and **2d** that are stabilized by 0–5 kcal mol$^{-1}$ ($\Delta H^{o} = \Delta H_{free}^{\ddagger} - \Delta H_{complex}^{\ddagger}$) relative to infinitely separated reactants; however, they are not minima on the free energy surface and thus are not expected to be experimentally stable. These computed activation energies are 6–8 kcal/mol too low when compared to activation energies determined experimentally by Moss and Krogh–Jespersen;[13] therefore, conclusions from these results should be taken with caution. An increase of 6–7 kcal mol$^{-1}$ in the distortion energies and a decrease of 4–5 kcal mol$^{-1}$ in the favorable (negative) interaction energies results in a substantial increase of the activation energies along the series **1a→1b→1c**. The carbene and

alkene contributions to the total distortion energies for **1a** and **1b** are within ~1 kcal mol$^{-1}$. As for reactions of $CF_2$ (**1c**), distortion of the alkene is the primary cause of the increase in $\Delta E_d^{\ddagger}$, as seen

**Table 1.1** Distortion/interaction energies (in kcal mol$^{-1}$) for cycloaddition transition structures computed at the M06–2X/6-31+G(d,p) level

| Carbene | Alkene | $\Delta E^{\ddagger}$ | $\Delta E_d^{\ddagger}$ total | $\Delta E_d^{\ddagger}$ carbene | $\Delta E_d^{\ddagger}$ alkene | $\Delta E_i^{\ddagger}$ |
|---|---|---|---|---|---|---|
| $CCl_2$ | c–Hex | –4.1 | 2.6 | 1.5 | 1.1 | –6.7 |
| CClF | c–Hex | –1.3 | 5.3 | 2.0 | 3.3 | –6.6 |
| $CF_2$ | c–Hex | 7.4 | 9.2 | 2.6 | 6.6 | –1.8 |
| $CCl_2$ | 1–Hex | –3.3 | 1.5 | 0.9 | 0.6 | –4.8 |
| CClF | 1–Hex | –0.9 | 3.4 | 1.5 | 1.9 | –4.3 |
| $CF_2$ | 1–Hex | 6.4 | 7.3 | 2.0 | 5.3 | –0.9 |
| $CCl_2$ | $C_2H_4$ | 0.1 | 1.7 | 0.8 | 0.9 | –1.6 |
| CClF | $C_2H_4$ | 3.3 | 3.1 | 1.2 | 1.9 | 0.2 |
| $CF_2$ | $C_2H_4$ | 10.3 | 5.8 | 1.5 | 4.3 | 4.5 |
| ClCOMe | $C_2H_4$ | 8.4 | 6.9 | 3.4 | 3.5 | 1.5 |
| FCOMe | $C_2H_4$ | 13.1 | 8.7 | 3.5 | 5.2 | 4.4 |
| $C(OMe)_2$ | $C_2H_4$ | 16.2 | 10.3 | 3.3 | 7.0 | 6.0 |
| $CCl_2$ | α–ClACN | –3.2 | 1.3 | 0.0 | 1.3 | –4.5 |
| CClF | α–ClACN | 0.0 | 2.5 | 0.2 | 2.3 | –2.5 |
| $CF_2$ | α–ClACN | 5.4 | 5.0 | 0.4 | 4.6 | 0.3 |
| ClCOMe | α–ClACN | 0.0 | 4.8 | 0.9 | 3.9 | –4.8 |
| FCOMe | α–ClACN | 3.4 | 6.1 | 1.0 | 5.1 | –2.7 |
| $C(OMe)_2$ | α–ClACN | 1.2 | 7.9 | 2.3 | 5.6 | –6.7 |

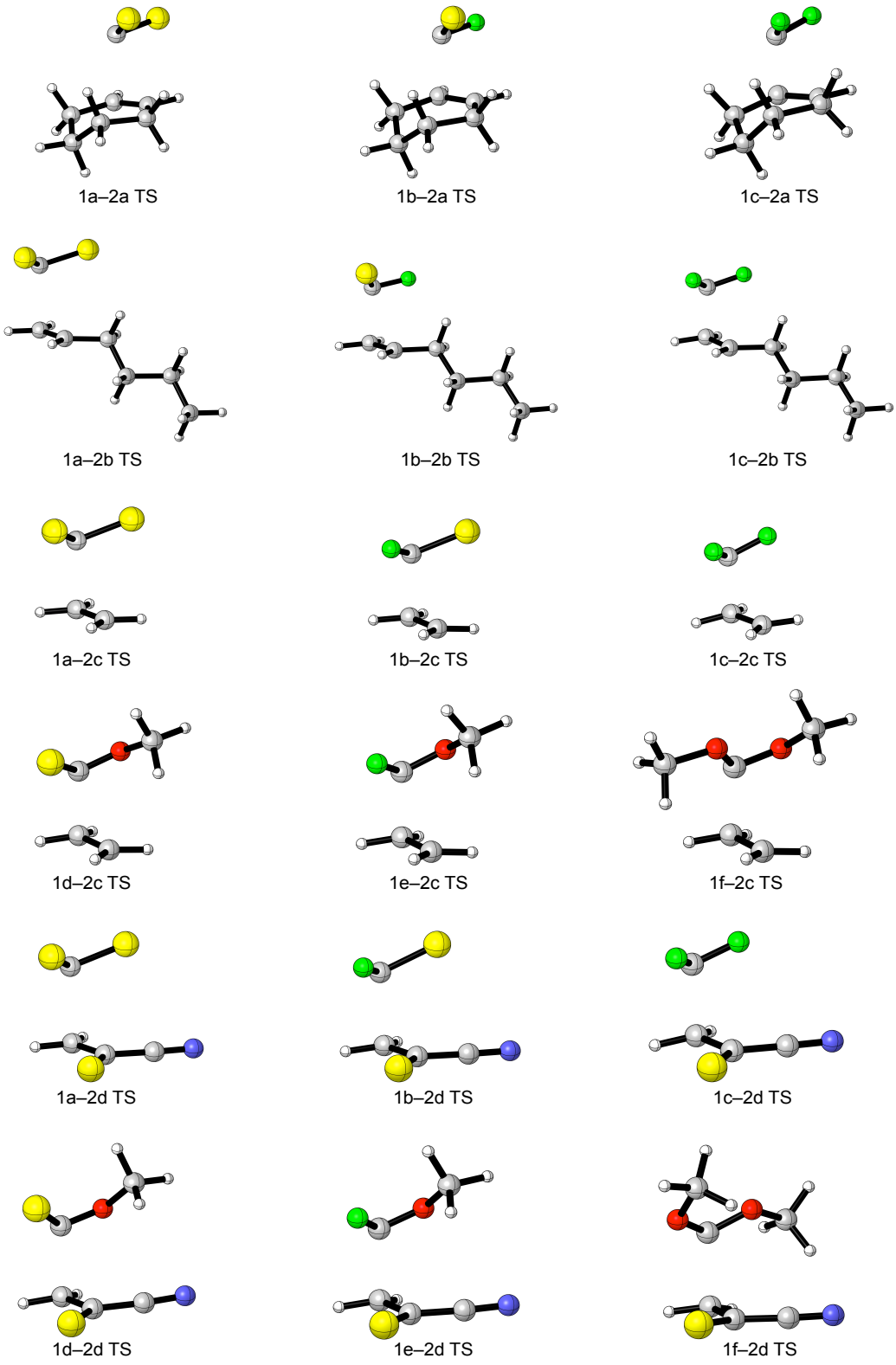


**Figure 1.2.** Optimized transition structures for the 18 cycloadditions in this study computed at the M06–2X/6–31+G(d,p) level. Geometrical parameters are given in Table 1.2.

in an average $\Delta\Delta E_{d,carbene}^{\ddagger}$ of 1.1 kcal mol$^{-1}$ and $\Delta\Delta E_{d,alkene}^{\ddagger}$ of 5.1 kcal mol$^{-1}$ relative to **1a**. Distortion of cyclohexene and 1–hexene comprises 42–72% and 40–73%, respectively, of the total distortion energy. In Table 1.2, the alkene bond distances, $r_{13}$, increase by a mere 0.02–0.03 Å from **1a→1b→1c**; therefore, C1–C3 bond elongation is not a significant contributor to $\Delta\Delta E_d^{\ddagger}$. We use angles $\alpha$ and $\beta$ to quantify the degree of pyramidalization of the terminal alkene carbons. As shown in Table 1.2, $\alpha$ increases by 17º and $\beta$ increases by 6º along the series **1a→1b→1c**. A greater extent of pyramidalization at C3 of the alkene occurs as a result of non–least motion approach in which the C2–C3 bond forms before the C2–C1 bond. We conclude that pyramidalization of the alkene carbons is the major distortion occurring at the transition state, and the change in C1–C3 bond length occurs mainly after the transition state. An increase in the values of $\alpha$ and $\beta$ indicates progressively later transition states and greater nucleophilic character of the carbene. The distance between C2 and the midpoint of the alkene ($d$) as well as the forming bond distances ($r_{12}$ and $r_{23}$) become shorter along the same series **1a→1b→1c**, which also supports later transition states and increasing $\Delta E_d^{\ddagger}$.

Based on the values of the carbene tilt angle $\gamma$ in Table 1.2,[8] **1a–c** react as electrophilic carbenes toward electron–rich alkenes **2a** and **2b**. Increasing carbene LUMO energies ($CCl_2$: -3.74 eV; CClF: –3.39 eV; $CF_2$: –2.83 eV)[13] lead to decreased overlap with the π–orbitals of **2a** and **2b**, which is likely one factor that attributes to a higher $\Delta E_i^{\ddagger}$ for **1c**. However, since $\Delta E_i^{\ddagger}$ for **1a** and **1b** are essentially identical, there must be a complex interplay of factors that render this analysis of $\Delta\Delta E_i^{\ddagger}$ incomplete. An energy decomposition analysis would be required for any greater insight into the physical origins of $\Delta E_i^{\ddagger}$.

**Table 1.2.** Geometrical parameters of the cycloaddition transition structures computed at the M06–2X/6–31+G(d,p) level. Distances are in Å and angles are in degrees

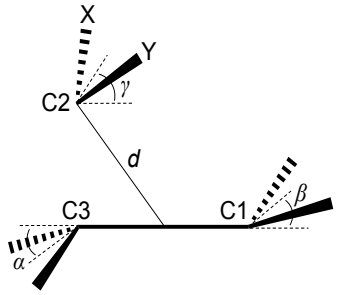


| Carbene | Alkene | $r_{12}$ | $r_{23}$ | $d$ | $r_{13}$ | ∠XCY | $\alpha$ | $\beta$ | $\gamma$ |
|---|---|---|---|---|---|---|---|---|---|
| $CCl_2$ | c–Hex | 2.60 | 2.28 | 2.35 | 1.36 | 108 | 9 | 1 | 31 |
| CClF | c–Hex | 2.41 | 1.99 | 2.10 | 1.37 | 105 | 18 | 2 | 35 |
| $CF_2$ | c–Hex | 2.29 | 1.81 | 1.94 | 1.38 | 104 | 26 | 7 | 39 |
| $CCl_2$ | 1–Hex | 2.79 | 2.34 | 2.49 | 1.35 | 108 | 6 | 3 | 35 |
| CClF | 1–Hex | 2.51 | 2.06 | 2.19 | 1.36 | 104 | 13 | 6 | 35 |
| $CF_2$ | 1–Hex | 2.39 | 1.81 | 2.01 | 1.38 | 104 | 23 | 9 | 41 |
| $CCl_2$ | $C_2H_4$ | 2.63 | 2.18 | 2.32 | 1.35 | 109 | 9 | 3 | 40 |
| CClF | $C_2H_4$ | 2.46 | 2.00 | 2.14 | 1.36 | 106 | 15 | 5 | 39 |
| $CF_2$ | $C_2H_4$ | 2.37 | 1.84 | 2.00 | 1.37 | 105 | 22 | 8 | 44 |
| ClCOMe | $C_2H_4$ | 2.47 | 1.92 | 2.10 | 1.37 | 113 | 20 | 4 | 48 |
| FCOMe | $C_2H_4$ | 2.42 | 1.84 | 2.04 | 1.38 | 110 | 24 | 5 | 50 |
| $C(OMe)_2$ | $C_2H_4$ | 2.45 | 1.83 | 2.05 | 1.39 | 111 | 28 | 7 | 57 |
| $CCl_2$ | α–ClACN | 2.82 | 2.29 | 2.48 | 1.35 | 110 | 11 | 5 | 42 |
| CClF | α–ClACN | 2.65 | 2.11 | 2.30 | 1.36 | 107 | 16 | 6 | 41 |
| $CF_2$ | α–ClACN | 2.52 | 1.93 | 2.14 | 1.37 | 106 | 24 | 8 | 44 |
| ClCOMe | α–ClACN | 2.63 | 2.04 | 2.25 | 1.37 | 114 | 21 | 8 | 50 |
| FCOMe | α–ClACN | 2.56 | 1.96 | 2.17 | 1.38 | 111 | 24 | 10 | 49 |
| $C(OMe)_2$ | α–ClACN | 2.64 | 2.01 | 2.24 | 1.38 | 112 | 25 | 11 | 55 |

**Cycloadditions to ethylene**

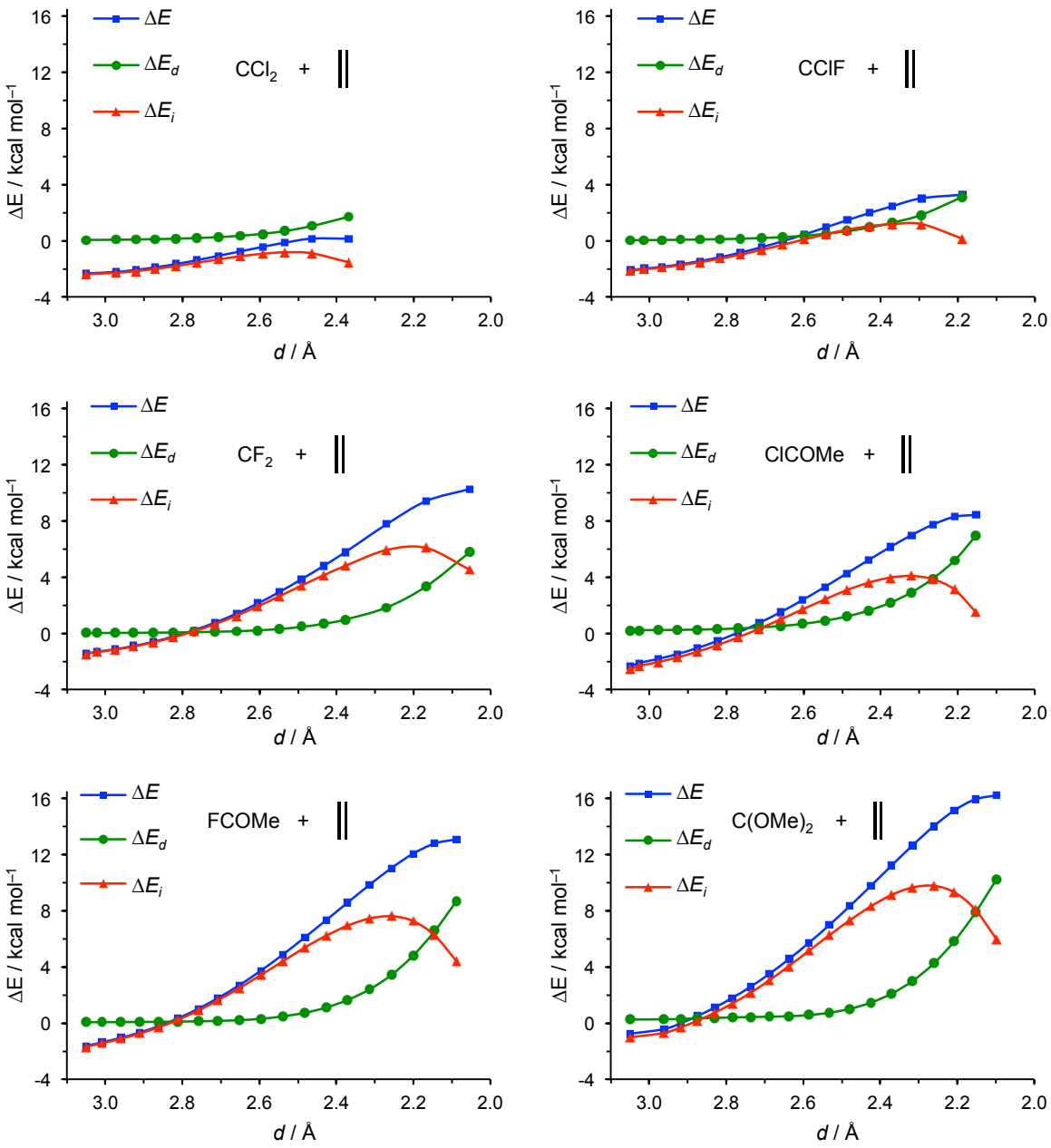


**Figure 1.3.** Distortion/interaction analysis of the (2+1) cycloaddition reaction between carbenes **1a–f** and **2c** projected onto the distance between C2 and the midpoint of ethylene (in Å). All data have been computed at the M06–2X/6–31+G(d,p) level.

In addition to the distortion/interaction analyses for the TS that are collected in Table 1.1, the reaction profiles together with their decomposition into $\Delta E_d$ and $\Delta E_i$ for cycloadditions of

dihalocarbenes **1a–c** and methoxycarbenes **1d–f** to ethylene (**2c**) are shown in Figure 1.3. Plots of $\Delta E_d$ and $\Delta E_i$ for all cycloadditions to **2c** are shown in Figures 1.4 and 1.5, respectively. Activation energies for cycloadditions of **1a–c** and **1d–f** to **2c** increase from 0–10 and 8–16 kcal

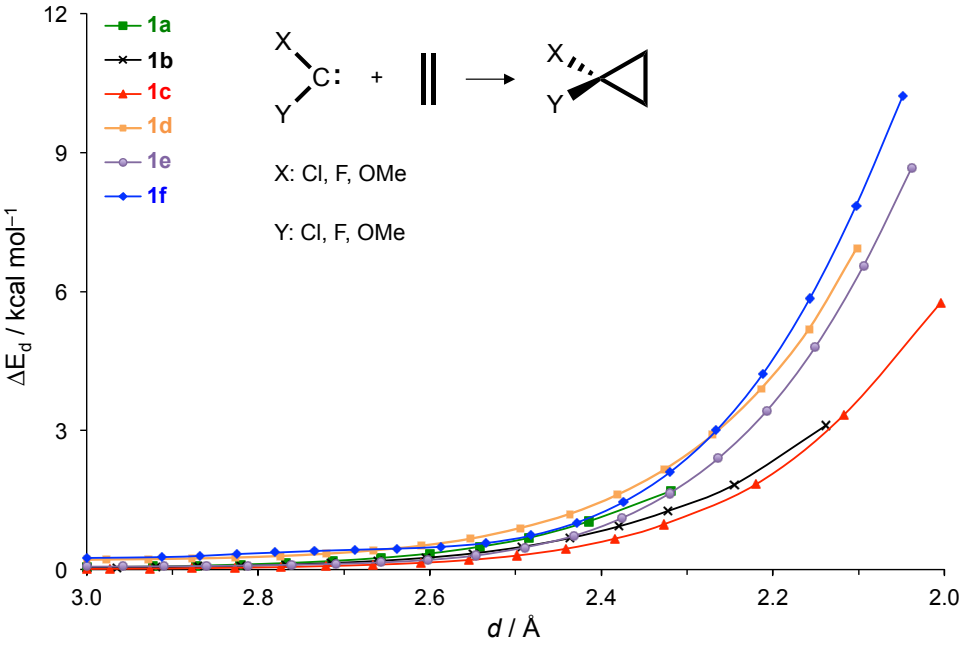


**Figure 1.4.** Distortion energy profiles of carbene cycloadditions to ethylene

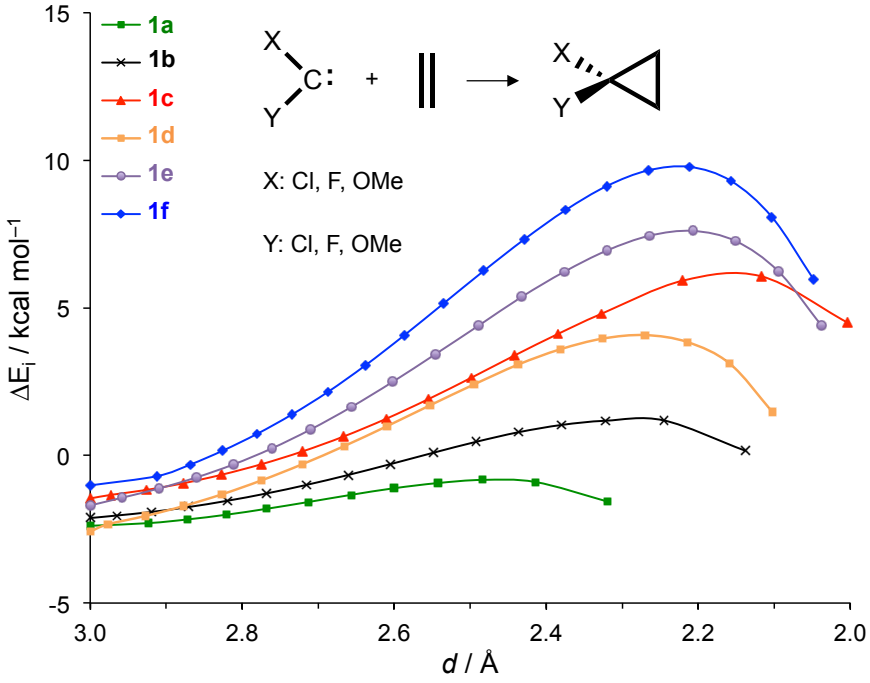


**Figure 1.5.** Interaction energy profiles of carbene cycloadditions to ethylene

mol$^{-1}$, respectively. Changes in $\Delta E_d^{\ddagger}$ and $\Delta E_i^{\ddagger}$ are comparable in magnitude, and both contribute to an increase in $\Delta E^{\ddagger}$ from **1a→1b→1c** and from **1d→1e→1f**. The distortion of ethylene comprises 51–74% of the total distortion energy. Carbene tilt angles in Table 1.2 indicate that **1a–c** are predominantly electrophilic and **1d–f** are predominantly nucleophilic in cycloadditions to **2c**. All interaction energies for the reactions with **2c** are positive except for that of **1a**, resulting in activation barriers greater than the inherent distortion in the transition structures. This result differs from those seen for example in 1,3-dipolar and Diels-Alder cycloadditions, where the interaction energies at the transition states are negative, i.e., favorable, in all cases such that the activation barrier is decreased relative to the distortion energy.[30] The alkyl substituents of **2a** and **2b** raise the HOMO of ethylene while the –Cl and –CN substituents of **2d** lower the LUMO of ethylene. Both of these perturbations decrease the frontier molecular orbital gaps between the carbene and alkene and lead to favorable interaction energies with respect to ethylene. Previously reported trends in HOMO and LUMO energies for these alkenes support this conclusion.[13] This trend in reactivity has been documented in the literature for other bimolecular reactions.[31-35] Houk and Ess examined cycloadditions of hydrazoic acid, an ambiphilic 1,3–dipole, to a series of substituted alkenes and found that electron–rich and electron–deficient alkenes lower the activation barriers ~2 kcal mol$^{-1}$ compared to ethylene.[30]

From the distortion/interaction analyses in Figure 1.3, medium–range ($d$ ~ 3 Å) attractive interactions exist while there is yet no distortion between the carbene and ethylene. This results in a negative $\Delta E$ relative to infinitely separated reactants and indicates formation of π-complexes, as mentioned earlier. In all cycloadditions to ethylene, there is no substantial increase in $\Delta E_d$ while d > 2.4 Å (Figure 1.3); therefore, the rise in $\Delta E$ along the reaction coordinate is primarily due to an increasingly destabilizing interaction between the carbene and the alkene. The early

inversion of $\Delta E_i$ from destabilizing to stabilizing in **1a** is responsible for a particularly early transition state. This behavior seems to be general to pericyclic reactions as it has been observed by Bickelhaupt in (3+2) cycloadditions,[36] Alder–ene reactions,[37] and double group–transfer reactions.[38] Bickelhaupt has also pointed out that the initially destabilizing $\Delta E_i$ observed in pericyclic reactions contrasts those seen in other bimolecular reactions such as $S_N2$ substitution[39] and E2 elimination.[40]

**Cycloadditions to α–chloroacrylonitrile**

The same general increase in $\Delta E^{\ddagger}$ from **1a→1b→1c** is observed with α–chloroacrylonitrile as in additions to **2a–c** due to increased stabilization of the carbene by fluorine substituents. The distortion of α–chloroacrylonitrile (**2d**) is the dominant factor of $\Delta E_d^{\ddagger}$, comprising 71–100% of the total distortion energy in the transition state. The activation energy of **1a** addition to **2d** is negative due to a favorable interaction energy of 4.5 kcal mol$^{-1}$ that compensates for the 1 kcal mol$^{-1}$ distortion energy of **2d** in the transition state. The computed activation barrier of –3.2 kcal/mol for the cycloaddition of **1a** to **2d** is substantially lower than the experimentally determined value of 5.4 kcal/mol.[13] There is a dramatic increase in reactivity of **1d–f** toward **2d** as compared to **2c** ($\Delta\Delta E^{\ddagger}$ ranges from 8–15 kcal mol$^{-1}$). These differences are caused by large favorable changes in interaction energy and relatively small unfavorable changes in distortion energy of the **2d** series relative to **2c**: average values of $\Delta\Delta E_d^{\ddagger}$ and $\Delta\Delta E_i^{\ddagger}$ for cycloadditions of **1d–f** to **2c** and **2d** are +2.4 and –8.7 kcal mol$^{-1}$ respectively. Cycloadditions of **1c** and **1d** to **2d** have the same amount of distortion in the TS; thus, the higher reactivity of **1d** relative to **1c** is a result of a 5 kcal mol$^{-1}$ difference in $\Delta E_i^{\ddagger}$.

We investigated the relationship between the distortion energies and activation energies as was done previously for other cycloaddition reactions.[41–43] Houk and Ess discovered a linear

correlation between activation energy and distortion energy in the transition states for 18 1,3-dipolar cycloadditions.[30] Houk and co–workers also observed a similar correlation for 1,4-dihydrogenations and Diels–Alder cycloadditions of aromatic molecules.[41] Figure 1.6 shows a plot of $\Delta E^{\ddagger}$ versus $\Delta E_d^{\ddagger}$ for the cycloadditions to ethylene and α–chloroacrylonitrile. The observed correlation ($r^2$ = 0.95) for cycloadditions to **2c** indicates that the increasing activation barrier is a direct result of increasing distortion energy in the transition state. The cooperative increase in $\Delta E_i^{\ddagger}$ as shown in Table 1.1 results in the same correlation ($r^2$ = 0.95) between $\Delta E^{\ddagger}$ and $\Delta E_i^{\ddagger}$ for additions to **2c** (Figure S–1.1). Therefore, activation energies for cycloadditions of **1a–f** to **2c** are equally controlled by both $\Delta E_d^{\ddagger}$ and $\Delta E_i^{\ddagger}$. Similarly, $\Delta E_d^{\ddagger}$ and $\Delta E_i^{\ddagger}$ exert equal control of $\Delta E^{\ddagger}$ for cycloadditions of **1a–c** to **2a** and **2b** with $r^2$ ~ 0.95–0.99 (not shown). For cycloadditions to **2d**, there is essentially no correlation ($r^2$ = 0.38) between $\Delta E^{\ddagger}$ and $\Delta E_d^{\ddagger}$ for the complete carbene set; however, a correlation does exist for the dihalocarbenes **1a–c** ($r^2$ = 1).

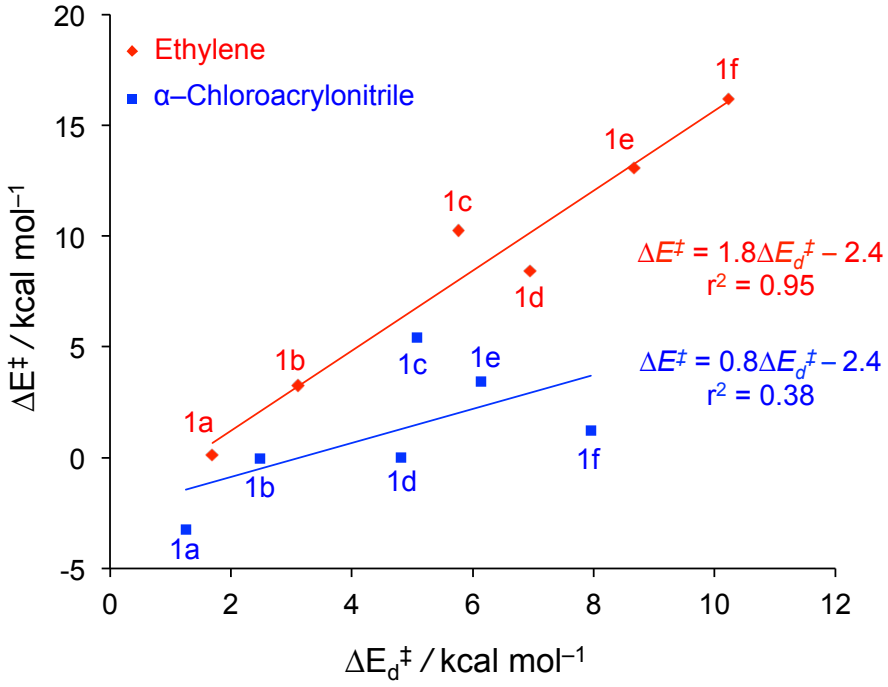


**Figure 1.6.** Plot of activation energy versus distortion energy for carbene cycloadditions to ethylene (**2c**; red diamonds) and α–chloroacrylonitrile (**2d**; blue squares).

## Conclusions

Generally, it is observed that pyramidalization of the alkene carbons is the primary contributor to $\Delta E_d^{\ddagger}$ in carbene cycloadditions. When compared to dihalocarbenes **1a** and **1b**, cycloadditions of **1c** to all four alkenes show anomalously unfavorable interaction energies in the transition state. Cycloadditions of **1b** and **1c** with **2c** have essentially the same distortion energy profile, as seen in Figure 1.4; therefore, the higher $\Delta E^{\ddagger}$ of the latter is the result of a later transition state originating from more destabilizing $\Delta E_i$ throughout the reaction. $\Delta E_d^{\ddagger}$ is constant for the reactions of **1c** and **1d** to **2d**, so a more favorable $\Delta E_i^{\ddagger}$ relative to **1c** is responsible for the higher reactivity of **1d**. The cycloaddition of $C(OMe)_2$ to α–chloroacrylonitrile shows a $\Delta E_i^{\ddagger}$ that is more favorable than expected (**1f** + **2d**; Table 1.1) and contributes to a breakdown in the correlation between $\Delta E^{\ddagger}$ and $\Delta E_d^{\ddagger}/\Delta E_i^{\ddagger}$ observed for **2a–c**. These results suggest that (2+1) cycloadditions are not only distortion–controlled as are other pericyclic reactions. As represented in Figures 1.4 and 1.5, small differences in distortion energies but large differences in interaction energies control the position of the transition state and the reaction rate.

## References


1. Hoffmann, R. *J. Am. Chem. Soc.* **1968**, *90*, 1475–1485. http://dx.doi.org/10.1021/ja01008a016

2. Woodward, R. B.; Hoffmann, R. *Angew. Chem. Int. Ed.* **1969**, *8*, 781–853 and references cited therein. http://dx.doi.org/10.1002/anie.196907811

3. Moore, W. R.; Moser, W. R.; LaPrade, J. E. *J. Org. Chem.* **1963**, *28*, 2200–2205. http://dx.doi.org/10.1021/jo01044a012

4. Bodor, N.; Dewar, M. J. S.; Wasson, J. S. *J. Am. Chem. Soc.* **1972**, *94*, 9095–9102. http://dx.doi.org/10.1021/ja00781a018

5. Hoffmann, R.; Hayes, D. M.; Skell, P. S. *J. Phys. Chem.* **1972**, *76*, 664–669. http://dx.doi.org/10.1021/j100649a010

6. Kollmar, H. J. *J. Am. Chem. Soc.* **1978**, *100*, 2660–2664.
http://dx.doi.org/10.1021/ja00477a015

7. Joo, H.; Kraka, E.; Quapp, W.; Cremer, D. *Mol. Phys.* **2007**, *105*, 2697–2717 and references cited therein.
http://dx.doi.org/10.1080/00268970701620677

8. Rondan, N. G.; Houk, K. N.; Moss, R. A. *J. Am. Chem. Soc.* **1980**, *102*, 1770–1776.
http://dx.doi.org/10.1021/ja00526a002

9. Moss, R. A.; Wang, L.; Zhang, M.; Skalit, C.; Krogh–Jespersen, K. *J. Am. Chem. Soc.* **2008**, *130*, 5634–5635.
http://dx.doi.org/10.1021/ja8005226
PMid:18393413

10. Moss, R. A.; Wang, L.; Krogh–Jespersen, K. *J. Am. Chem. Soc.* **2009**, *131*, 2128–2130.
http://dx.doi.org/10.1021/ja809370j
PMid:19173648

11. Moss, R. A.; Wang, L.; Zhang, M. *Org. Lett.* **2008**, *10*, 4045–4048.
http://dx.doi.org/10.1021/ol801575v
PMid:18729368

12. Moss, R. A.; Zhang, M.; Krogh–Jespersen, K. *Org. Lett.* **2010**, *12*, 3476–3479.
http://dx.doi.org/10.1021/ol1013119
PMid:20597479

13. Zhang, M.; Moss, R. A.; Thompson, J.; Krogh–Jespersen, K. *J. Org. Chem.* **2012**, *77*, 843–850.
http://dx.doi.org/10.1021/jo2023558
PMid:22204738

14. Ess, D. H.; Houk, K. N. *J. Am. Chem. Soc.* **2007**, *129*, 10646–10647.
http://dx.doi.org/10.1021/ja0734086
PMid:17685614

15. van Zeist, W.-J.; Bickelhaupt, F. M. *Org. Biomol. Chem.* **2010**, *8*, 3118–3127.
http://dx.doi.org/10.1039/b926828f
PMid:20490400

16. Zhao, Y.; Truhlar, D. G. *Theor. Chem. Account* **2008**, *120*, 215–241.
http://dx.doi.org/10.1007/s00214-007-0310-x

17. Frisch, M. J. *et al*. *Gaussian 09*, revision C–01; Gaussian, Inc.: Wallingford, CT, 2009 (see complete reference in the Supporting Information).

18. Fukui, K. *J. Phys. Chem.* **1970**, *74*, 4161–4163.
http://dx.doi.org/10.1021/j100717a029

19. Deng, L; Ziegler, T. *Int. J. Quantum Chem.* **1994**, *52*, 731–765.
http://dx.doi.org/10.1002/qua.560520406

20. Moss, R. A.; Lawrynowicz, W.; Turro, N. J.; Gould, I. R.; Cha, Y. *J. Am. Chem. Soc.* **1986**, *108*, 7028–7032. http://dx.doi.org/10.1021/ja00282a030

21. Houk, K. N.; Rondan, N. G.; Mareda, J. *J. Am. Chem. Soc.* **1984**, *106*, 4291–4293. http://dx.doi.org/10.1021/ja00327a052

22. Houk, K. N.; Rondan, N. G.; Mareda, J. *Tetrahedron* **1985**, *41*, 1555–1563. http://dx.doi.org/10.1016/S0040-4020(01)96395-1

23. Turro, N. J.; Lehr, G. F.; Butcher, J. A., Jr.; Moss, R. A.; Guo, W. *J. Am. Chem. Soc.* **1982**, *104*, 1754–1756. http://dx.doi.org/10.1021/ja00370a059

24. Moss, R. A.; Perez, L. A.; Turro, N. J.; Gould, I. R.; Hacker, N. P. *Tetrahedron Lett.* **1983**, *24*, 685-688. http://dx.doi.org/10.1016/S0040-4039(00)81498-7

25. Gould, I. R.; Turro, N. J.; Butcher, J. A., Jr., Doubleday, C. E., Jr., Hacker, N. P.; Lehr, G. F.; Moss, R. A.; Cox, D. P.; Guo, W.; Munjal, R. C.; Perez, L. A. Fedorynski, M. *Tetrahedron* **1985**, *41*, 1587–1600. http://dx.doi.org/10.1016/S0040-4020(01)96399-9

26. Liu, M. T. H. *J. Chem. Soc.*, *Chem. Commun.* **1985**, 982–985.

27. Liu, M. T. H.; Subramanian, R. *Tetrahedron Lett.* **1985**, *26*, 3071–3074. http://dx.doi.org/10.1016/S0040-4039(00)98621-0

28. Tomioka, H.; Hayashi, N.; Izawa, Y.; Liu, M. T. H. *J. Am. Chem. Soc.* **1984**, *106*, 454–456. http://dx.doi.org/10.1021/ja00314a051

29. Liu, M. T. H.; Subramanian, R. *J. Chem. Soc.*, *Chem. Commun.* **1984**, 1062–1064.

30. Ess, D. H.; Houk, K. N. *J. Am. Chem. Soc.* **2008**, *130*, 10187–10198. http://dx.doi.org/10.1021/ja800009z PMid:18613669

31. Huisgen, R. In *1,3–Dipolar Cycloaddition Chemistry*; Padwa, A., Ed.; John Wiley and Sons: New York, 1984; Vol. 1 and references cited therein.

32. Houk, K. N. In *1,3–Dipolar Cycloaddition Chemistry*; Padwa, A., Ed.; John Wiley and Sons: New York, 1984; Vol. 2 and references cited therein.

33. Houk, K. N.; Sims, J.; Duke, R. E., Jr.; Strozier, R. W.; George, J. K. *J. Am. Chem. Soc.* **1973**, *95*, 7287–7301. http://dx.doi.org/10.1021/ja00803a017

34. Houk, K. N.; Sims, J.; Watts, C. R.; Luskus, L. J. *J. Am. Chem. Soc.* **1973**, *95*, 7301–7315. http://dx.doi.org/10.1021/ja00803a018

35. Bastide, J.; Ghandour, W. E.; Henri–Rousseau, O. *Tetrahedron Lett.* **1972**, *13*, 4225–4228. http://dx.doi.org/10.1016/S0040-4039(01)94281-9

36. Fernandez, I.; Bickelhaupt, F. M.; Cossio, F. P. *J. Org. Chem.* **2011**, *76*, 2310–2314. http://dx.doi.org/10.1021/jo102572x PMid:21388217

37. Fernandez, I.; Bickelhaupt, F. M. *J. Comput. Chem.* **2012**, *33*, 509–516. http://dx.doi.org/10.1002/jcc.22877 PMid:22144106

38. Fernandez, I.; Bickelhaupt, F. M.; Cossio, F. P. *Chem. Eur. J.* **2009**, *15*, 13022–13032. http://dx.doi.org/10.1002/chem.200902024 PMid:19852009

39. Bento, P. A.; Bickelhaupt, F. M. *J. Org. Chem.* **2008**, *73*, 7290–7299. http://dx.doi.org/10.1021/jo801215z PMid:18690745

40. Bickelhaupt, F. M. *J. Comput. Chem.* **1999**, *20*, 114–128. http://dx.doi.org/10.1002/(SICI)1096-987X(19990115)20:1<114::AID-JCC12>3.0.CO;2-L

41. Hayden, A. E.; Houk, K. N. *J. Am. Chem. Soc.* **2009**, *131*, 4084–4089. http://dx.doi.org/10.1021/ja809142x PMid:19256544

42. Liang, Y.; Mackey, J. L.; Lopez, S. A.; Liu, F.; Houk, K. N. *J. Am. Chem. Soc.* **2012**, *134*, 17904–17907. http://dx.doi.org/10.1021/ja809142x

43. Lopez, S. A.; Houk, K. N. *J. Org. Chem.* **2013**, *78*, 1778–1783. http://dx.doi.org/10.1021/jo301267b PMid:22764840

## II. Computed Activation Parameters of Carbene Cycloadditions Relative to Carbene-Alkene Complexes, Pyridinium Ylides, and Diazirine Ylides

### Introduction

Carbenes experience stabilization relative to methylene upon mixing of a lone pair from π-donor substituents with the vacant p-orbital of the carbene. The σ orbital remains unmixed; therefore, the result is an increased HOMO-LUMO gap.[1] A later transition state for cycloadditions to alkenes occurs due to a less stabilizing carbene LUMO-alkene HOMO interaction, which gives a higher activation energy. In addition, a larger HOMO-LUMO gap achieved by this type of orbital interaction results in carbenes that shift from reacting as electrophiles with electron-rich alkenes to reacting as nucleophiles with electron-deficient alkenes. Moss and Krogh-Jespersen separately used laser flash photolysis and electronic structure theory calculations to determine the activation parameters for a series of cycloadditions of carbenes to alkenes.[2] Their experiments and computations show that $\Delta H^{\ddagger}$ of the carbene cycloadditions increase with the stability of the carbene under consideration, in accord with numerous past investigations.[3–8] Intriguingly, reciprocal behavior of $\Delta H^{\ddagger}$ and $-T\Delta S^{\ddagger}$ is observed in experiments while parallel behavior is observed in computations. Computational determination of the contributions from entropy to the activation free energies are substantially more unfavorable than experimental data suggests, which directly results in an overestimation of $\Delta G^{\ddagger}$. Perhaps more surprisingly, experiments indicate that $-T\Delta S^{\ddagger}$ is more favorable in the later, tighter transition states involving more stable carbenes. A viable explanation for the difference between computed and measured activation parameters of (2+1) cycloadditions of singlet carbenes to alkenes is lacking. Moss and Krogh-Jespersen[9] and others[10–12] propose that this discrepancy is at least in part due to restriction of translational and rotational motions in the condensed phase. This effect was recently observed through kinetic experiments of

phenylchlorocarbene addition to tetramethylethylene in pentane, octane, and decane solvents. A decrease in $-T\Delta S^{\ddagger}$ was observed with the increase in solvent chain length, which was rationalized as an increase in accessible solvent surface area resulting in the formation of more stabilizing solvent cages. This hypothesis cannot be tested with electronic structure theory calculations in the gas phase or with implicit solvation models, and in fact computational results were in opposition to experiment for this reaction.[13]

Another possible explanation for the large computed errors in $-T\Delta S^{\ddagger}$ for carbene cycloadditions is the reversible formation of carbene-alkene precursor complexes. The existence of intermediate complexes in the cycloadditions of singlet carbenes to alkenes has been proposed[14–18] and debated[19,20] in the past. Intrinsically, there is an entropic penalty to form a bimolecular complex in which the carbene and alkene both lose translational and rotational degrees of freedom. The resulting computed values of $\Delta S^{\ddagger}$ of carbene cycloadditions relative to these precursor complexes should be substantially lower than ~40 eu as seen in gas phase bimolecular reactions relative to infinitely separated reactants. Moss used UV–Vis spectroscopy and varying levels of theory to characterize π– and *O*–ylidic complexes of carbenes with aryl ethers.[21] He determined that binding enthalpies of the complexes are small while large unfavorable entropies result in positive free energies. Moss and Krogh–Jespersen propose the possibility that weakly bound π–complexes are formed in some carbene cycloadditions. They located $CCl_2$ and CClF complexes to cyclohexene and 1-hexene with the B3LYP, MPW1K, and MPW1PW91 functionals and the 6-311+G(d) basis set;[9] however, no experimental or computational evidence of precursor complexes exists for the cycloadditions of $CF_2$, ClCOMe, FCOMe, or $C(OMe)_2$. Herein, we report a computational investigation of carbene-alkene precursor complex formation for 18 cycloadditions, which consist of the cycloadditions of

dihalocarbenes (**1a–c**) to cyclohexene (**2a**) and 1–hexene (**2b**), as well as the cycloadditions of **1a–f** to ethylene (**2c**) and α-chloroacrylonitrile (ClACN: **2d**) (Figure 2.1).

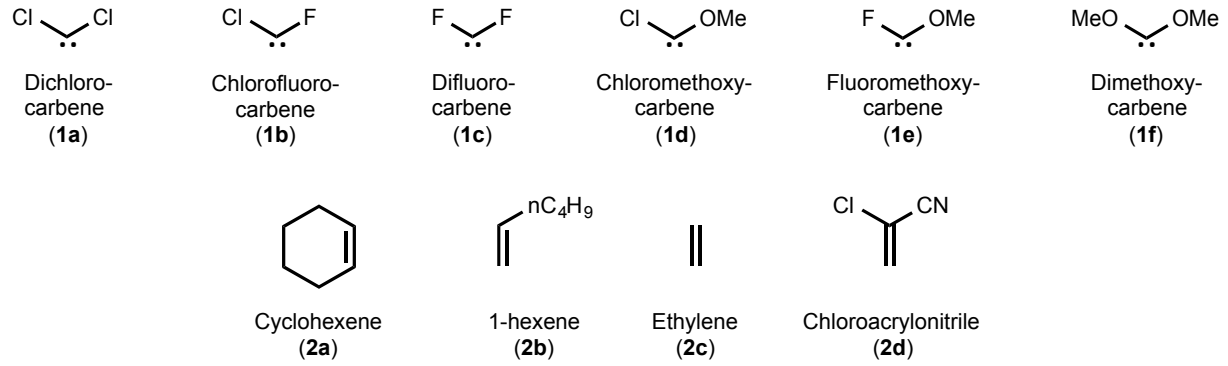


**Figure 2.1.** The carbenes and alkenes employed in this computational study.

Moss uses the pyridine ylide method[22] to experimentally determine the rate constants for carbene cycloadditions to alkenes. Briefly, the apparent rate of pyridinium ylide formation in pentane decreases upon the addition of an alkene at a constant concentration of pyridine. A correlation of the observed rate constants for the formation of pyridinium ylide vs. [alkene] is linear, and its slope gives the rate for the addition of carbene to the alkene. Although the concentration of pyridine in these experiments is low, we investigated the possibility of carbene cycloaddition coupled to the loss of carbene from pyridine, as shown in Scheme 2.1. Our hypothesis was that some of the entropic penalty of the direct carbene cycloaddition to an alkene would be counteracted by an increase in entropy of pyridine as a result of C-N bond dissociation in the transition state. This reaction is also entropically favorable from a fundamental thermodynamic standpoint, since it represents a bimolecular reaction that produces two products instead of only one.

For experimental determination of activation parameters for carbene cycloadditions, the carbenes were generated by photolysis of diazirine precursors. Liu et al. studied singlet carbenes with varying electronic properties and structures and obtained spectroscopic evidence of the

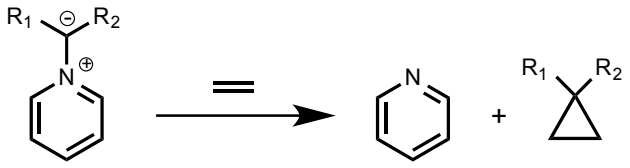

**Scheme 2.1.** Proposed carbene cycloaddition to ethylene through a pyridinium ylide.

formation of carbene-diazirine ylides with subsequent decomposition to azines (Scheme 2.2 – top). He concluded that the "existence of a carbene-diazirine ylide as an intermediate on the way to azine seems to be a general phenomenon for carbenes with a singlet ground state."[23] The singlet character of the carbenes investigated here has been confirmed.[9] Consequently, we have used quantum mechanical calculations to explore the possibility of carbene cycloaddition coupled to the loss of carbene from diazirine precursor (Scheme 2.2 – down arrow). This reaction should be entropically more favorable than the reaction of free carbene to alkene for the same reasons as the pyridinium ylide reaction noted in Scheme 2.1.

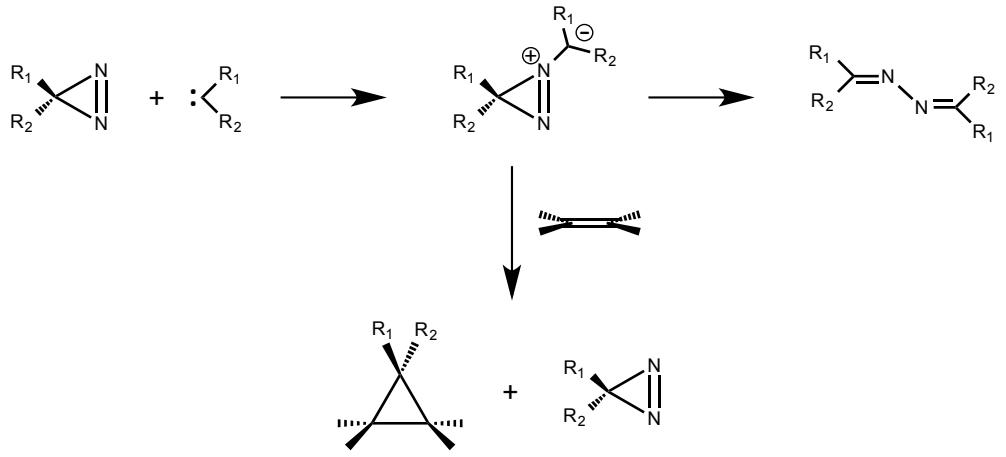

**Scheme 2.2.** Formation of a carbene-diazirine ylide followed by either decomposition into an azine or formal addition of carbene to an alkene.

**Computational Methodology**

Gas phase reactants, intermediates, and transition states were optimized using tight convergence criteria and an ultrafine integration grid at the M06–2X/6–31+G(d,p)[24,25] level.

Analytical frequencies were computed mostly with the rigid-rotor/harmonic oscillator approxmation. In specific cases, the quasiharmonic approximation of Truhlar[26,27] was applied to adjust the entropic contribution of rotational/vibrational modes below 100 $cm^{-1}$ while in other cases the partition functions were computed with anharmonic frequencies and rotational/vibrational coupling. All reported potential energy minima have positive definite Hessian matrices and all transition structures have only one negative eigenvalue in their diagonalized force constant matrices. Intrinsic Reaction Coordinate (IRC)[28,29] calculations were performed on all transition structures to verify that they connect the appropriate reactants and products on the potential energy surface. Carbene-alkene precursor complexes were located by optimizing the final structure toward the reactant side of each IRC calculation. The effect of solvation in pentane on the energetics of these carbene cycloadditions was tested implicitly with the SMD model. An extended investigation of the cycloadditions to **2d** was conducted with optimizations and frequencies obtained at the B97D/6-31+G(d,p), B3LYP-D3/def2-QZVP, and MP2/6-311+G(2d,p) levels of theory as well as single point energies at the CCSD(T)/cc-pVTZ//MP2/6-311+G(2d,p) level. These results are available in the Supporting Information. All computations were performed with the Gaussian 09 suite of programs.[25]

## Results and Discussion

### Carbene-alkene precursor complexes.

Activation barriers for carbene cycloadditions to cyclohexene, 1-hexene, ethylene, and α-chloroacrylonitrile computed in this work are compared to previous computations and experimental data, upon availability, in Table 2.1. The activation parameters in this work were computed at the M06–2X/6–31+G(d,p) level while previous computations were conducted at the B3LYP/6–311+G(d) level. Table 2.2 displays a comparison between our computed activation

parameters, with reference to infinitely separated reactants and carbene-alkene precursor complexes, to experimental data. In the cycloadditions of **2a** and **2b**, there is an increase in $\Delta H^{\ddagger}$ from **1a→1c** that qualitatively agrees both with experiment and with previous computations. Our computations underestimate the experimental values of $\Delta H^{\ddagger}$ by about 1–3 kcal/mol for additions of **1a** and **1b** to **2a** and **2b**, while additions of **1c** to **2a** and **2b** are overestimated by 2–5 kcal/mol.

**Table 2.1.** Activation parameters for carbene cycloadditions computed at the M06–2X/6–31+G(d,p) level of theory (this work) and at the B3LYP/6–311+G(d) level of theory (previous work). Experimental data are included. All values are in kcal/mol.

| Carbene | Alkene | This work | | | Previous work | | | Experimental data | | |
|---|---|---|---|---|---|---|---|---|---|---|
| | | $\Delta H^{\ddagger}$ | $-T\Delta S^{\ddagger}$ | $\Delta G^{\ddagger}$ | $\Delta H^{\ddagger}$ | $-T\Delta S^{\ddagger}$ | $\Delta G^{\ddagger}$ | $\Delta H^{\ddagger}$ | $-T\Delta S^{\ddagger}$ | $\Delta G^{\ddagger}$ |
| **1a** | **2a** | -1.7 | 12.7 | 10.4 | 1.3 | 12.1 | 13.5 | 3.3 | 3.1 | 6.4 |
| **1b** | **2a** | 1.0 | 12.7 | 13.7 | 3.9 | 12.7 | 16.6 | 5.0 | 2.3 | 7.3 |
| **1c** | **2a** | 9.5 | 12.3 | 21.8 | – | – | – | 6.3 | 1.3 | 7.6 |
| **1a** | **2b** | -0.9 | 12.5 | 11.6 | 1.2 | 11.4 | 12.6 | 4.1 | 3.4 | 7.5 |
| **1b** | **2b** | 1.5 | 13.2 | 14.7 | 3.3 | 12.2 | 15.5 | 5.4 | 2.3 | 7.7 |
| **1c** | **2b** | 8.3 | 12.8 | 21.1 | – | – | – | 7.4 | 1.1 | 8.6 |
| **1a** | **2c** | 3.1 | 10.5 | 13.6 | – | – | – | – | – | – |
| **1b** | **2c** | 5.4 | 11.1 | 16.5 | – | – | – | – | – | – |
| **1c** | **2c** | 11.1 | 11.8 | 22.9 | – | – | – | – | – | – |
| **1d** | **2c** | 11.6 | 12.0 | 23.6 | – | – | – | – | – | – |
| **1e** | **2c** | 16.3 | 12.3 | 28.6 | – | – | – | – | – | – |
| **1f** | **2c** | 18.5 | 12.4 | 30.9 | – | – | – | – | – | – |
| **1a** | **2d** | -1.1 | 12.3 | 11.2 | 0.5 | 9.3 | 9.8 | 4.8 | 2.7 | 7.5 |
| **1b** | **2d** | 1.7 | 12.8 | 14.5 | – | – | – | – | – | – |
| **1c** | **2d** | 7.2 | 12.3 | 19.5 | – | – | – | – | – | – |
| **1d** | **2d** | 3.3 | 13.5 | 16.8 | 6.8 | 10.4 | 17.2 | 3.4 | 6.0 | 9.4 |
| **1e** | **2d** | 7.2 | 13.5 | 20.7 | 9.0 | 10.2 | 19.2 | 5.4 | 5.1 | 10.5 |
| **1f** | **2d** | 6.2 | 13.5 | 19.7 | 10.0 | 11.2 | 21.2 | 6.9 | 2.8 | 9.7 |

There is a 4–8 kcal/mol jump in $\Delta H^{\ddagger}$ from **1b→1c** for all alkenes in this study. In a related study, computations showed that high barriers for cycloadditions of $CF_2$ relative to $CCl_2$ and CClF are due to unfavorable interaction energies;[30] however, the fundamental cause of the large deviation from experiment remains unclear. Large unfavorable entropies of activation for

cycloadditions of **1a–c** to **2a–b** relative to infinitely separated reactants result in computed values of $\Delta G^{\ddagger}$ that are larger than experimental values by 4–14 kcal/mol. The agreement between computed and experimental values of $-T\Delta S^{\ddagger}$ and $\Delta G^{\ddagger}$ considerably improves when considering carbene-alkene precursor complexes, although the activation free energy is still overestimated in **1c** + **2a/2b**.

**Table 2.2.** Activation parameters for carbene cycloadditions relative to separated reactants and carbene-alkene precursor complexes computed at the M06–2X/6–31+G(d,p) level of theory. Experimental data are included. All values are in kcal/mol.

| Carbene | Alkene | Separated reactants | | | Precursor complexes | | | Experimental data | | |
|---|---|---|---|---|---|---|---|---|---|---|
| | | $\Delta H^{\ddagger}$ | $-T\Delta S^{\ddagger}$ | $\Delta G^{\ddagger}$ | $\Delta H^{\ddagger}$ | $-T\Delta S^{\ddagger}$ | $\Delta G^{\ddagger}$ | $\Delta H^{\ddagger}$ | $-T\Delta S^{\ddagger}$ | $\Delta G^{\ddagger}$ |
| **1a** | **2a** | -1.7 | 12.7 | 10.4 | 1.2 | 1.9 | 3.1 | 3.3 | 3.1 | 6.4 |
| **1b** | **2a** | 1.0 | 12.7 | 13.7 | 4.0 | 2.4 | 6.4 | 5.0 | 2.3 | 7.3 |
| **1c** | **2a** | 9.5 | 12.3 | 21.8 | 11.8 | 2.9 | 14.6 | 6.3 | 1.3 | 7.6 |
| **1a** | **2b** | -0.9 | 12.5 | 11.6 | 1.3 | 1.8 | 3.1 | 4.1 | 3.4 | 7.5 |
| **1b** | **2b** | 1.5 | 13.2 | 14.7 | 3.4 | 2.4 | 5.8 | 5.4 | 2.3 | 7.7 |
| **1c** | **2b** | 8.3 | 12.8 | 21.1 | 9.8 | 3.0 | 12.8 | 7.4 | 1.1 | 8.6 |
| **1a** | **2c** | 3.1 | 10.5 | 13.6 | 3.7 | 2.9 | 6.5 | – | – | – |
| **1b** | **2c** | 5.4 | 11.1 | 16.5 | 5.9 | 3.2 | 9.1 | – | – | – |
| **1c** | **2c** | 11.1 | 11.8 | 22.9 | 12.7 | 2.6 | 15.3 | – | – | – |
| **1d** | **2c** | 11.6 | 12.0 | 23.6 | 11.2 | 3.1 | 14.4 | – | – | – |
| **1e** | **2c** | 16.3 | 12.3 | 28.6 | 5.5 | 1.0 | 6.5 | – | – | – |
| **1f** | **2c** | 18.5 | 12.4 | 30.9 | 6.2 | 1.0 | 7.2 | – | – | – |
| **1a** | **2d** | -1.1 | 12.3 | 11.2 | 2.9 | 1.7 | 4.6 | 4.8 | 2.7 | 7.5 |
| **1b** | **2d** | 1.7 | 12.8 | 14.5 | 5.5 | 1.0 | 6.5 | – | – | – |
| **1c** | **2d** | 7.2 | 12.3 | 19.5 | 9.6 | 2.6 | 12.1 | – | – | – |
| **1d** | **2d** | 3.3 | 13.5 | 16.8 | 5.6 | 1.8 | 7.4 | 3.4 | 6.0 | 9.4 |
| **1e** | **2d** | 7.2 | 13.5 | 20.7 | 8.1 | 1.9 | 10.0 | 5.4 | 5.1 | 10.5 |
| **1f** | **2d** | 6.2 | 13.5 | 19.7 | 8.4 | 2.1 | 10.5 | 6.9 | 2.8 | 9.7 |

There are no experimental results for the cycloadditions of **1a–f** to **2c**. Nonetheless, our computed activation parameters shown in Table 2.1 suggest the feasibility of these reactions at 298 K. The activation energies for the cycloadditions of $CCl_2$ and $CF_2$ to ethylene have been computed at the MP2/3-21G level to be -9.8 and 13.7 kcal/mol, respectively.[31] As in

cycloadditions to **2a** and **2b**, the barriers of cycloaddition to **2c** increase from **1a→1c** and along **1d→1f** with respect to infinitely separated reactants. The activation barriers of cycloadditions of methoxycarbenes **1d–f** to **2c** are less regular when starting from complexes, however. Both $\Delta H^{\ddagger}$ and $\Delta G^{\ddagger}$ for the cycloadditions of **1e** and **1f** to **2c** are anomalously low, and the entropy is the least unfavorable of all reactions studied.

In cycloadditions to α–chloroacrylonitrile, we observed an increase in $\Delta H^{\ddagger}$ and $\Delta G^{\ddagger}$ for the dihalocarbenes **1a–c** and for the methoxycarbenes **1d–f**. For the cycloadditions of methoxycarbenes **1d–f** relative to infinitely separated reactants, $\Delta H^{\ddagger}$ and $\Delta G^{\ddagger}$ increase initially from **1d** to **1e** as expected; however, the cycloaddition of dimethoxycarbene **1f** to **2d** is shown to be more facile than **1e**. The trend in our computed values of $\Delta G^{\ddagger}$ qualitatively agrees with experiment, but not for the same reason. Again, compensation between $\Delta H^{\ddagger}$ and $-T\Delta S^{\ddagger}$ is observed experimentally, whereas our computations show that a change in $\Delta H^{\ddagger}$ dominates the trend in $\Delta G^{\ddagger}$ while $-T\Delta S^{\ddagger}$ for **1d–f** remain the same. On the other hand, a high degree of accuracy in $\Delta G^{\ddagger}$ is obtained when considering carbene-alkene precursor complexes in the cycloadditions of **1d–f** to **2d**.

To provide a clear picture of the correlation between computed and experimental activation parameters, three graphs that incorporate the data from Table 2.2 are shown in Figure 2.2. In each plot, the blue circles represent computed activation parameters relative to infinitely separated reactants while the red squares represent those relative to carbene-alkene precursor

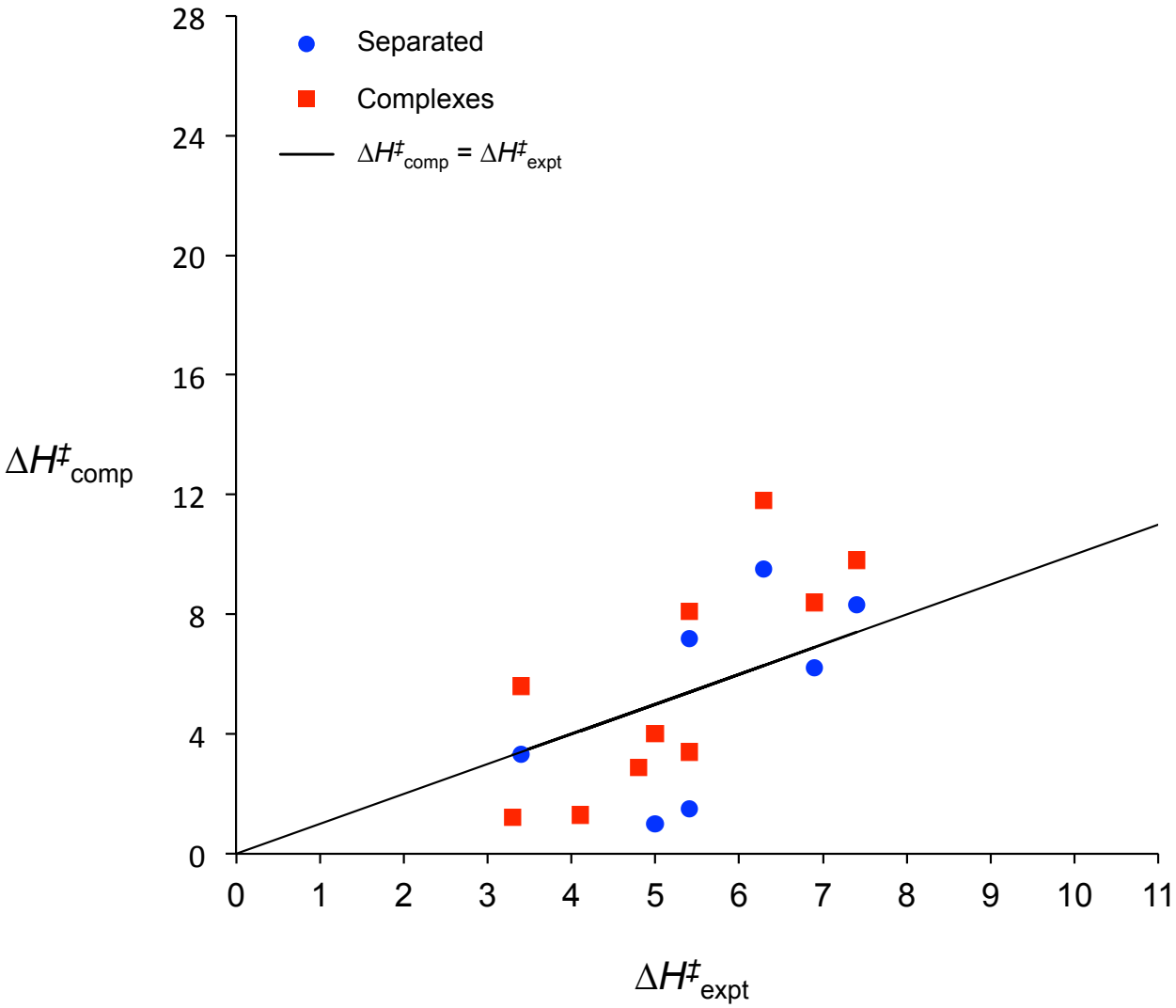
Separated
Complexes
$\Delta H^{\ddagger}_{comp} = \Delta H^{\ddagger}_{expt}$
$\Delta H^{\ddagger}_{comp}$
$\Delta H^{\ddagger}_{expt}$
0
4
8
12
16
20
24
28
0
1
2
3
4
5
6
7
8
9
10
11

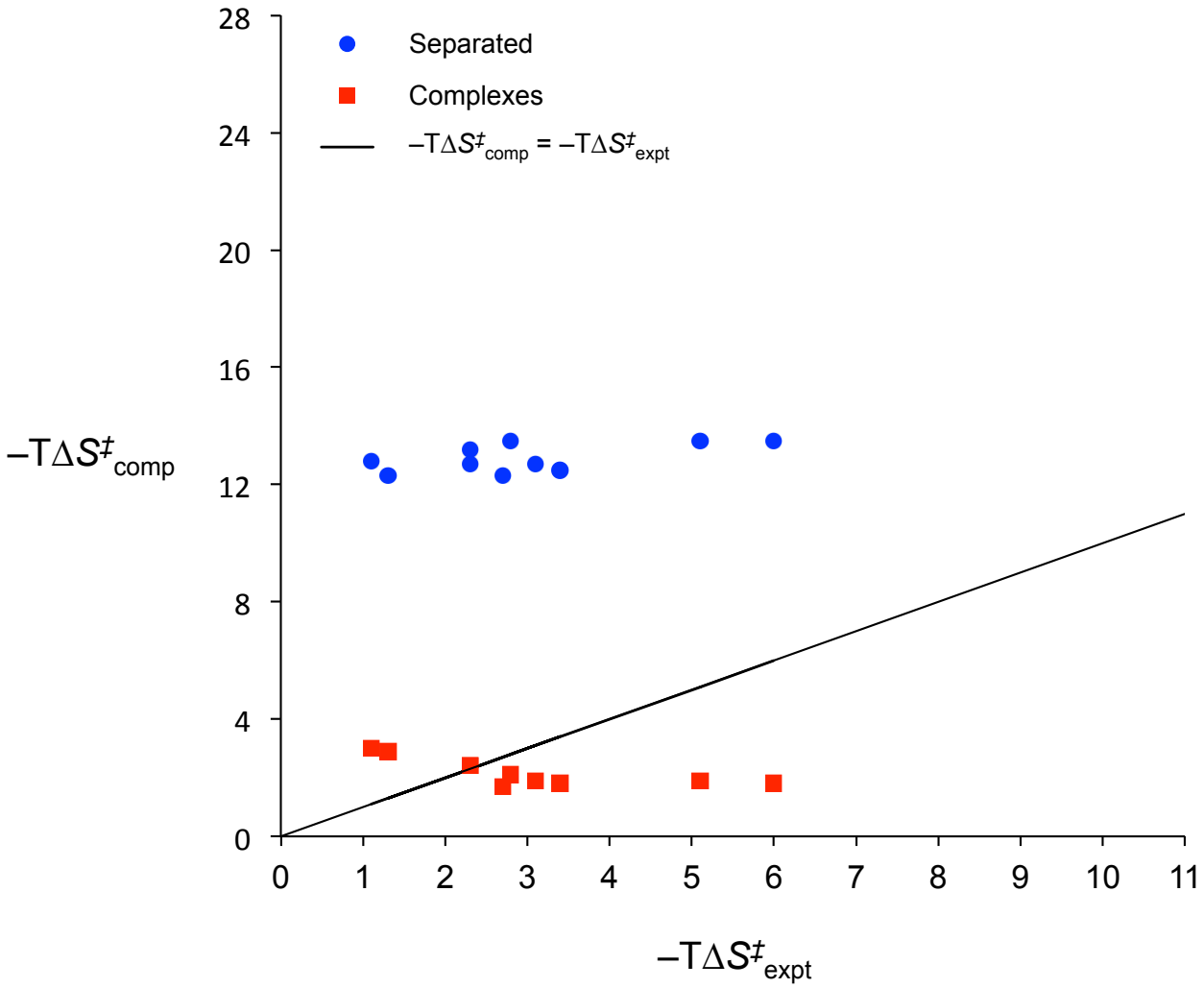
Separated
Complexes
$-T\Delta S^{\ddagger}_{comp} = -T\Delta S^{\ddagger}_{expt}$
$-T\Delta S^{\ddagger}_{comp}$
$-T\Delta S^{\ddagger}_{expt}$
0
4
8
12
16
20
24
28
0
1
2
3
4
5
6
7
8
9
10
11

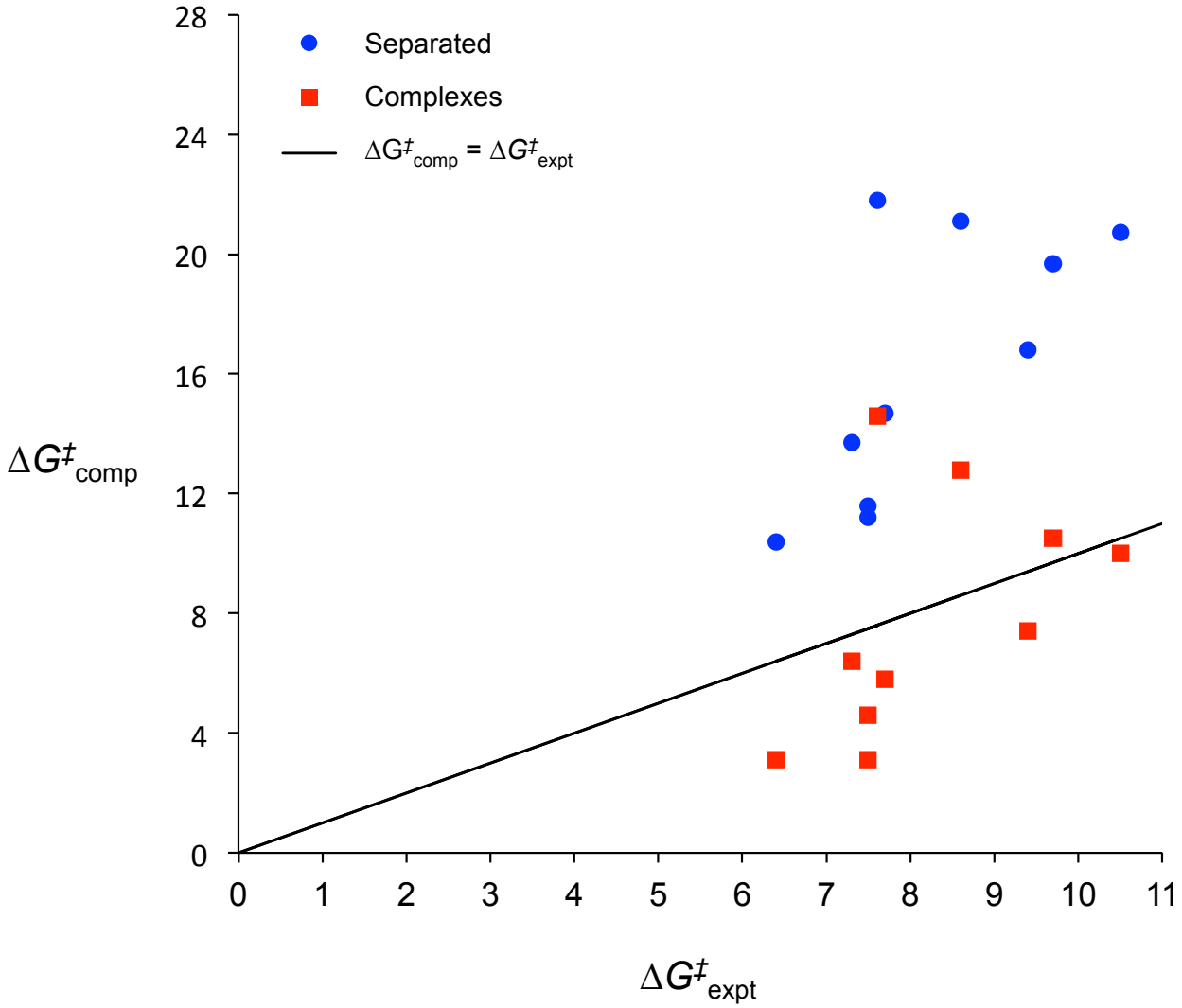


**Figure 2.2.** Comparisons of computed and experimental activation parameters for carbene cycloadditions. In each plot, the solid line is a hypothetical representation of perfect correlation.

complexes. The solid lines represent a hypothetical scenario in which theory matches experiment exactly. It can be seen clearly that the computed values of $-T\Delta S^{\ddagger}$ are constant in both cases even though the observed experimental values have a range of 5 kcal/mol. This figure illustrates the inadequacy of theory to accurately calculate the activation entropies of bimolecular reactions in solution. In $\Delta G^{\ddagger}$, there is virtually no correlation in either case; however, a comparison of all

three plots shows that $\Delta G^{\ddagger}$ computed relative to infinitely separated reactants is overestimated relative to experiment because of overestimation in $-T\Delta S^{\ddagger}$ as stated previously.

Figure 2.3 shows complexes formed between dihalocarbenes **1a–c** and cyclohexene **2a** and 1–hexene **2b** optimized at the M06–2X/6–31+G(d,p) level of theory. In these systems, the bisector of the carbene is slightly rotated with respect to the alkene π–bond such that one of the carbene bonds is eclipsing the alkene π–bond. The plane of the carbene is nearly parallel with the plane of the π–bond and there is no distortion, i.e. pyramidalization, of the alkene carbons. The lengths of the forming C–C bonds in the complexes generally increase in the order **1a** < **1b** < **1c**, suggesting earlier complex formation. This trend is opposite in the respective cycloaddition transition structures in which forming C–C bond distances decrease in the order **1a** > **1b** > **1c**.[30] Thus, the increase in $-T\Delta S^{\ddagger}$ down the series as shown by our computations is the result of earlier complexes with more vibrational and rotational degrees of freedom that must be constrained to tighter transition state structures. In fact, there are many reports in the literature of difficulties in calculating correct entropies of bimolecular reactions in solution, and we have encountered an especially pathological case.

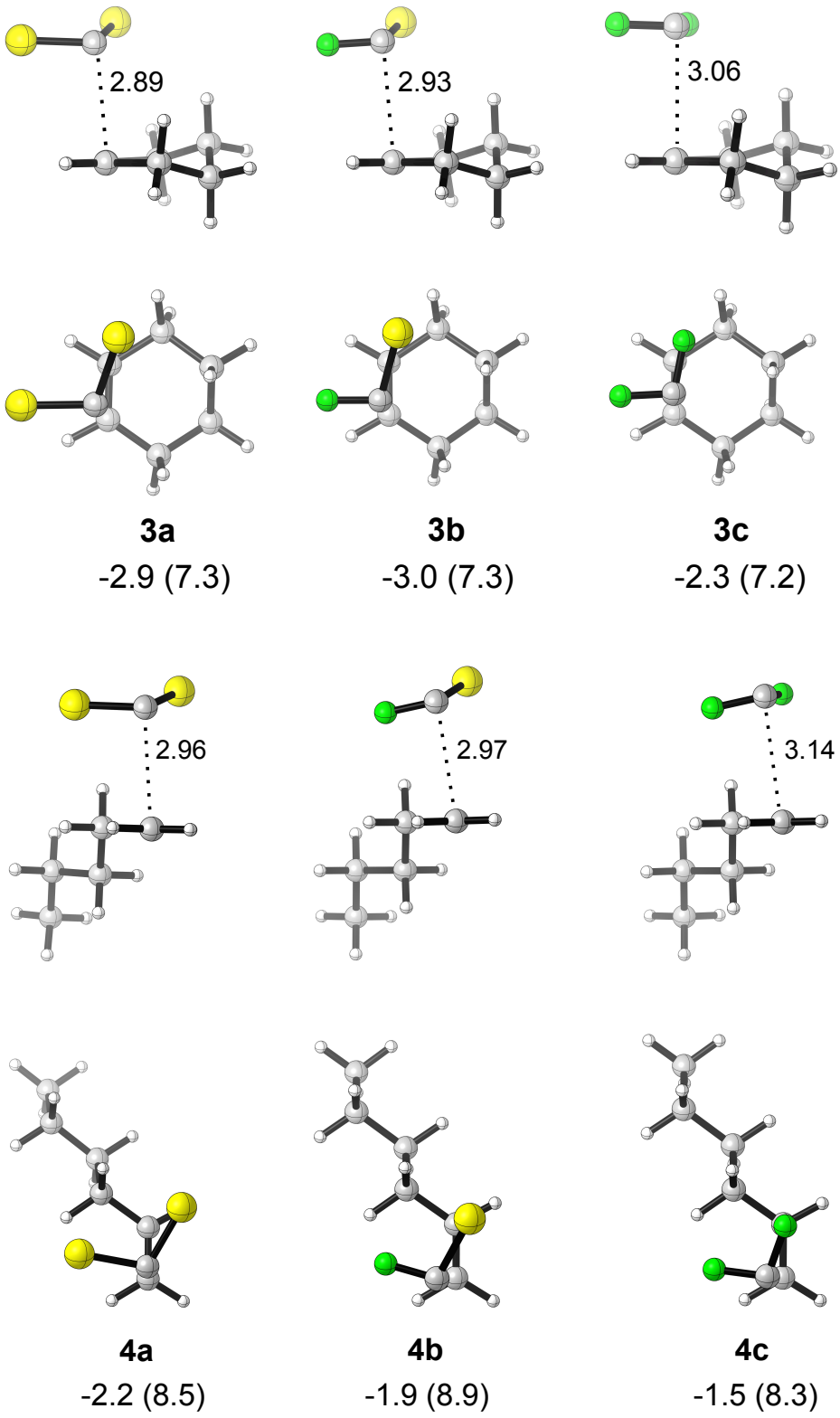


**Figure 2.3.** Carbene-alkene precursor complexes between dihalocarbenes **1a–c** and cyclohexene **2a** (top) and 1–hexene **2b** (bottom). Values of ΔH° (ΔG°) are at the M06–2X/6–31+G(d,p) level of theory. Distances are in Å.

The structures of π–complexes formed in the cycloadditions of **1a–f** to ethylene are shown in Figure 2.4. The complexes of **1a–c** and **2c** possess a high degree of symmetry with the carbene carbons directly above the alkene carbons and all of the forming bond lengths are essentially the same. The carbene bisectors are parallel to the ethylene bond axes. As in the complexes with **2a** and **2b**, the carbenes in these complexes are predominantly parallel to the ethylene plane and the ethylene is undistorted; however, ethylene is appreciably distorted from planarity in the complexes of **1e** and **1f**. Because alkene distortion is the primary contributor to the activation energy in carbene cycloadditions,[30] this early distortion in the complexes of **1e** and **1f** is likely responsible for the low values of $\Delta H^{\ddagger}$ for this cycloaddition (Table 2.2).

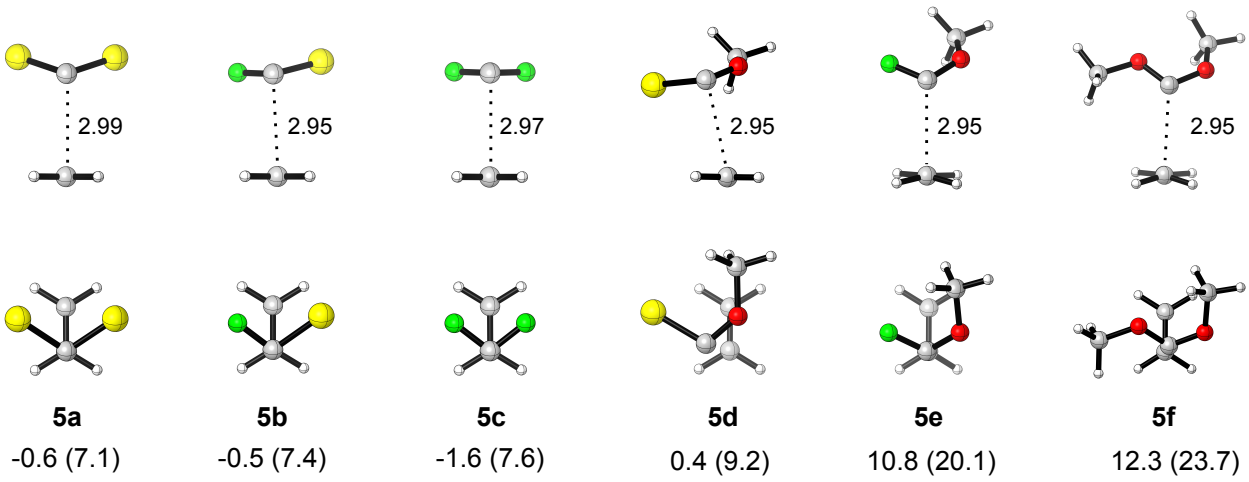


**Figure 2.4.** Side and overhead views of precursor complexes between carbenes **1a–f** and **2d**. Values of ΔH° (ΔG°) are at the M06–2X/6–31+G(d,p) level of theory and distances are in Å.

The structures of π–complexes **6a–f** formed in the cycloadditions of **1a–f** to α–chloroacrylonitrile are shown in Figure 2.5. The complex of **1a** and **2d** has similar characteristics as the complex of **1a** and **2c**, the major difference being that the latter is a looser complex ($\Delta r_{12}$ = 0.21 Å; $\Delta r_{23}$ = 0.13 Å). Unlike all other complexes located for these carbene cycloadditions, the complex between **1f** and **2d** is characterized by an electrostatic dipole–dipole interaction assisted

by electron donation into the C2–H σ* orbital as opposed to early carbene/alkene FMO overlap. Brinker et al. first observed this type of noncovalent interaction in the cycloaddition reactions of 7–norbornenylidene to acrylonitrile, fumaronitrile, and tricyanoethylene that resulted in 7–12 kcal/mol of stabilization in $\Delta E^{\circ}$ relative to separated reactants. Additionally, the latter two complexes were shown to be free energy minima.[32] The C3–H•••C2 distance is 2.45 Å, essentially in the middle of the range of interaction distances for the complexes computed by

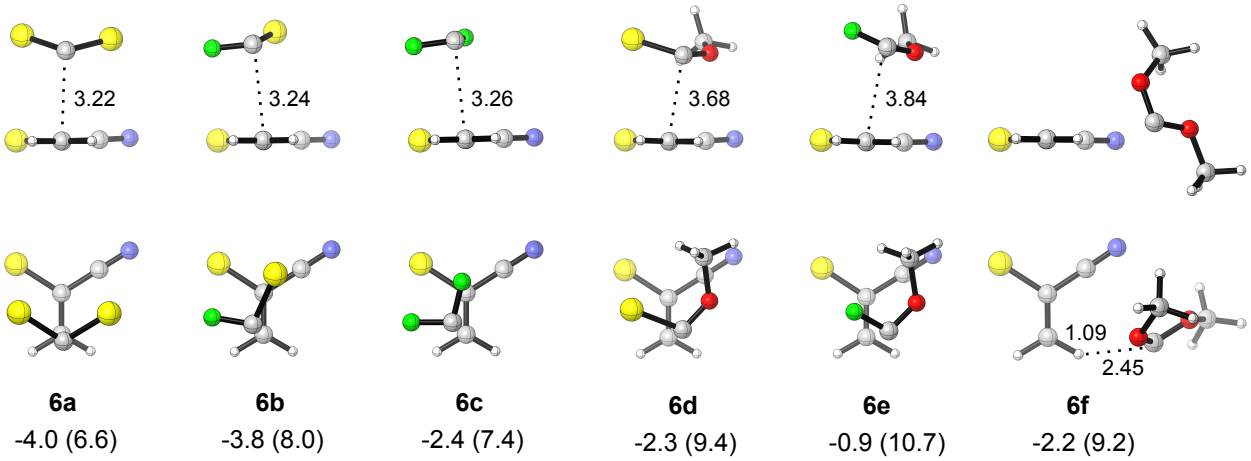


**Figure 2.5.** Side and overhead views of precursor complexes between carbenes **1a–f** and **2d**. Values of $\Delta H$ ($\Delta G$) are at the M06–2X/6–31+G(d,p) level of theory and distances are in Å.

Brinker (2.10–2.93 Å). At 1.09 Å, the C3–H bond length is only stretched by 0.01 Å relative to the ground state of **2d**. The complex observed between **1f** and **2d** results in activation barriers that are essentially the same as those in **1f** + **2d** ($\Delta\Delta H^{\ddagger}$ = 0.3 kcal/mol, $-T\Delta\Delta S^{\ddagger}$ = 0.2 kcal/mol, $\Delta\Delta G^{\ddagger}$ = 0.5 kcal/mol). Our results for the computed activation barriers of **1d–f** to **2d** show the best agreement with available experimental data, further implicating the existence of carbene–alkene precursor complexes and their role in the kinetics of carbene cycloadditions. While these complexes are stable in terms of potential energy relative to infinitely separated reactants, they exhibit positive free energies of formation. Complexes between $CCl_2$/$CF_2$ and ethylene have

previously been computed to be higher in free energy than separated reactants.[31] A summary of computed thermodynamics for the formation of carbene-**2d** precursor complexes at various levels of theory is shown in Figure 2.6. These large destabilization free energies as well as the absence of a transition state between separated reactants and complexes suggest that experimental observation of these computed complexes is not possible.

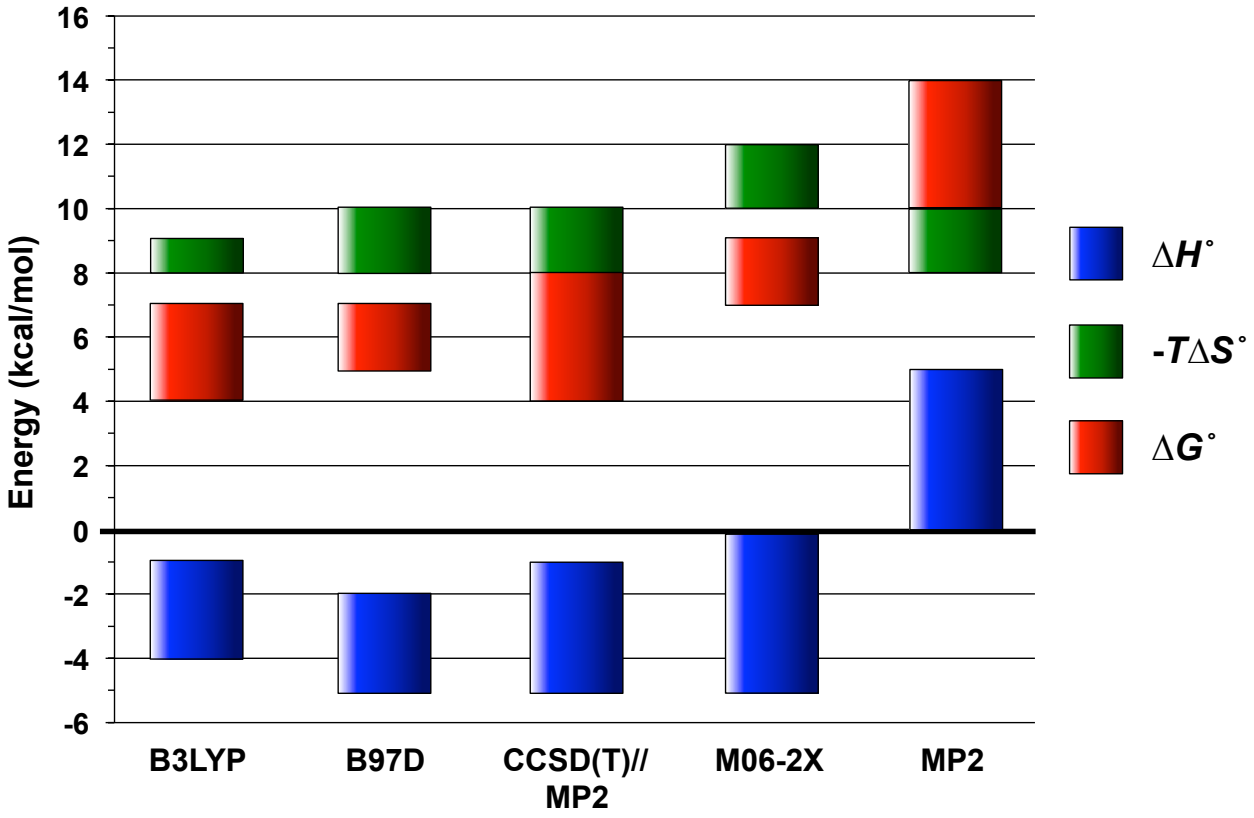


**Figure 2.6.** Summary of the thermodynamics of precursor complexes **6a–f** at various levels of theory.

Data sets containing a variety of noncovalent complexes have been developed and extensively benchmarked with high-level computational methods like CCSD(T)/CBS that are capable of producing interaction energies with "chemical accuracy," or errors less than 1 kcal/mol (for example, see reference 33 and references cited therein). Enthalpies and free energies of complex formation are less prevalent in computational literature however, as far as

we are aware, with some notable examples.[21,34] As a proof of principle, we sought examples of complex formation for which kinetic data are available and tested the capability of theory to reproduce the results. Briegleb obtained thermodynamic parameters for complexes of chloranil, picric acid, trinitrobenzene, and tetracyanoethylene with hexamethylbenzene.[35,36] The geometries of these complexes, optimized with B97D/6-31+G(d,p) and implicitly including the effects of $CCl_4$ with the SMD solvation model, are shown in Figure 2.7 along with experimental and computed free energies, enthalpies, and entropies of formation. Notable agreement exists between experimental and theoretical free energies of complex formation; however, closer

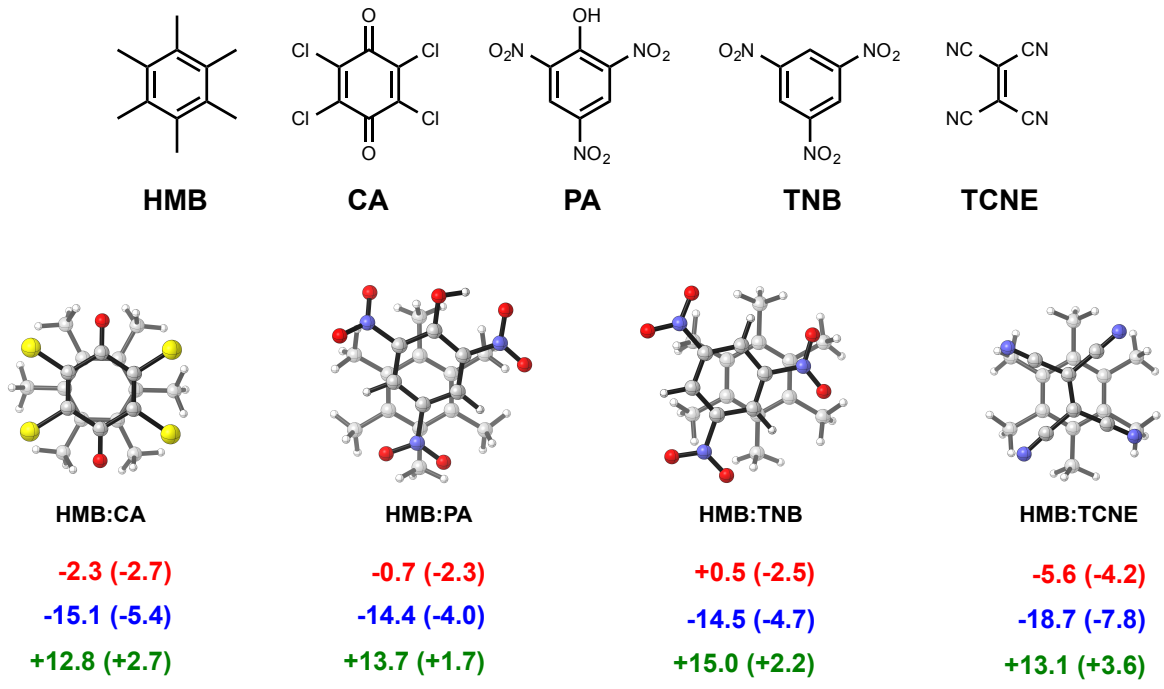


**Figure 2.7.** Optimized structures of π–complexes of chloranil (CA), picric acid (PA), trinitrobenzene (TNB), and tetracyanoethylene (TCNE) with hexamethylbenzene (HMB). Values are in kcal/mol at the B97D/6–31+G(d,p)/SMD level of theory and experimental values are in parentheses.

inspection of the data show that this agreement in the free energies results from fortuitous cancellation of errors ≥ 10 kcal/mol in the computed enthalpies and entropies of formation.

Obtaining reliable free energies with theory requires the accurate description of intermolecular and intramolecular interactions, which is dependent on the QM method, and adequate sampling of all relevant conformational degrees of freedom.[37,38] Therefore, the large overestimation of binding enthalpies in these complexes is the result of factoring in attractive dispersion forces while not compensating for the basis set superposition error of an incomplete and rather small basis set. The neglect of sampling protocol undoubtedly contributes to the overestimation of $-T\Delta S$ observed in the π-complexes of Figure 2.7 and possibly to the carbene-alkene precursor complexes as well.

Figure 2.8 shows one example each of several conceivable 1:1 π-complexes between chlorotrifluoromethylcarbene and isoquinoline and between chloromethylcarbene and anisole computed at the M06–2X/6-31+G(d,p) level of theory. Moss monitored the formation of a $ClCCF_3$-isoquinoline ylide by UV absorbance at 404 nm as a means of measuring the activation parameters for cycloadditions of $ClCCF_3$ to tetramethylethylene, cyclohexene, and 1-hexene.[39] Our calculations show a large binding enthalpy and a greater entropic penalty in the formation of this complex. Moss does not indicate the formation of this complex and the computed $\Delta G$ suggests that only about 2.4 % is present at equilibrium with free carbene and isoquinoline at 298 K. Moss computes several examples of weakly-bound complexes between $ClCCH_3$ and anisole at the PBEPBE/6-311+G(d) level of theory. Upon laser flash photolysis of the $ClCCH_3$ diazirine precursor, a peak in the UV/Vis spectrum dominates at 368 nm that is assigned to this complex.[40] Based on our computed $\Delta G$, this complex is present at an equilibrium concentration of 0.02 % with respect to free carbene and anisole, which is below the sensitivity of UV/Vis spectroscopy. Overall, it seems that there is a systematic error in the frequency corrections of complexes as

computed by standard electronic structure theory methods leading to high values of $-T\Delta S$ and $\Delta G$.

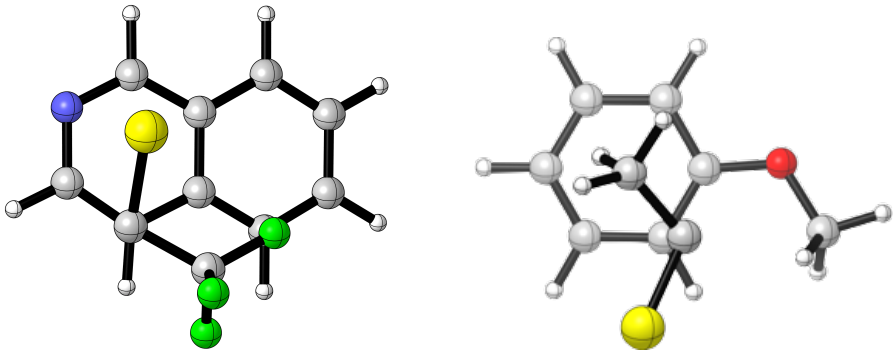


**Figure 2.8.** Optimized structures of π–complexes between chlorotrifluoromethylcarbene and isoquinoline and chloromethylcarbene and anisole. Values are $\Delta H$ ($\Delta G$) in kcal/mol at the M06–2X/6-31+G(d,p) level of theory.

**Table 2.3.** Comparison of $\Delta G$ and $\Delta G^{\ddagger}$ for carbene-alkene precursor complexes and transition states in the cycloaddition of $CCl_2$ + ethylene computed in the gas phase with the standard rigid-rotor/harmonic oscillator approximation, the quasiharmonic correction, and anharmonic frequencies with rovibrational coupling. Values are in kcal/mol at the M06-2X/6-31+G(d,p) level of theory.

| | Separated Reactants | Precursor Complex | Cycloaddition TS |
|---|---|---|---|
| **1a** + **2c** | 0.0 | 7.1 | 13.6 |
| **1a** + **2c** (QH) | 0.0 | 7.4 | 11.8 |
| **1a** + **2c** (anharmonic) | 0.0 | 6.3 | 11.5 |

The noncovalent complexes computed here all contain low frequency modes that, when using the standard rigid-rotor/harmonic oscillator model, lead to unphysical contributions to the entropy. To address this issue, we first applied the quasiharmonic correction of Truhlar to

arbitrarily raise all low modes up to a threshold value of 100 $cm^{-1}$. Second, we computed anharmonic frequencies and contributions from vibrational-rotational coupling in the cycloaddition of $CCl_2$ with ethylene. Neither one of these measures appreciably changed the consensus that complexes are predicted not to exist at an appreciable concentration or determine the kinetics of cycloaddition due to positive free energies of formation. A summary of these results, computed at the M06-2X/6-31+G(d,p) level of theory, is shown in Table 2.3. A slight improvement of the computational overestimation of $-T\Delta S^{\ddagger}$ is observed with the quasiharmonic correction and with the consideration of anharmonic frequencies relative to the standard model ($\Delta\Delta G^{\ddagger} \sim 2$ kcal/mol); however, this change is too small to correct the general disagreement between experiment and theory regarding the activation parameters of carbene cycloadditions.

**Pyridinium ylide formation.**

Since the formation of pyridinium ylides is integral to the experimental determination of kinetics in these cycloadditions, we decided to explore the potential for these ylides to play a direct role in carbene additions to alkenes. Values of $\Delta H$ and $\Delta G$ for $CCl_2$-pyridinium ylide formation were previously computed to be –30.0 kcal/mol and –19.9 kcal/mol at the PBEPBE/6-311+G(d) level of theory.[40] Computations at the M06-2X/6-31+G(d,p) level give comparable values of $\Delta H$ and $\Delta G$ of –31.2 kcal/mol and –19.0 kcal/mol. Figure 2.9 shows the computed enthalpy and free energy surfaces for the formation and addition of $CCl_2$-pyridinium ylide to ethylene.

The barriers for $CCl_2$ cycloaddition to ethylene through a $CCl_2$-pyridinium ylide are larger than through the direct addition of $CCl_2$. As seen in Table 2.1, $\Delta H^{\ddagger}$ of $CCl_2$ addition to ethylene is 3.1 kcal/mol or 3.7 kcal/mol relative to free carbene or ethylene complex respectively, whereas analogous values for the addition of $CCl_2$ through a pyridinium ylide intermediate are computed

to be 27.3 kcal/mol or 31.6 kcal/mol. The free energy of activation for the addition depicted in Figure 2.9 is 35.1 kcal/mol, which is larger than the addition of free $CCl_2$ by 21.5 kcal/mol, and

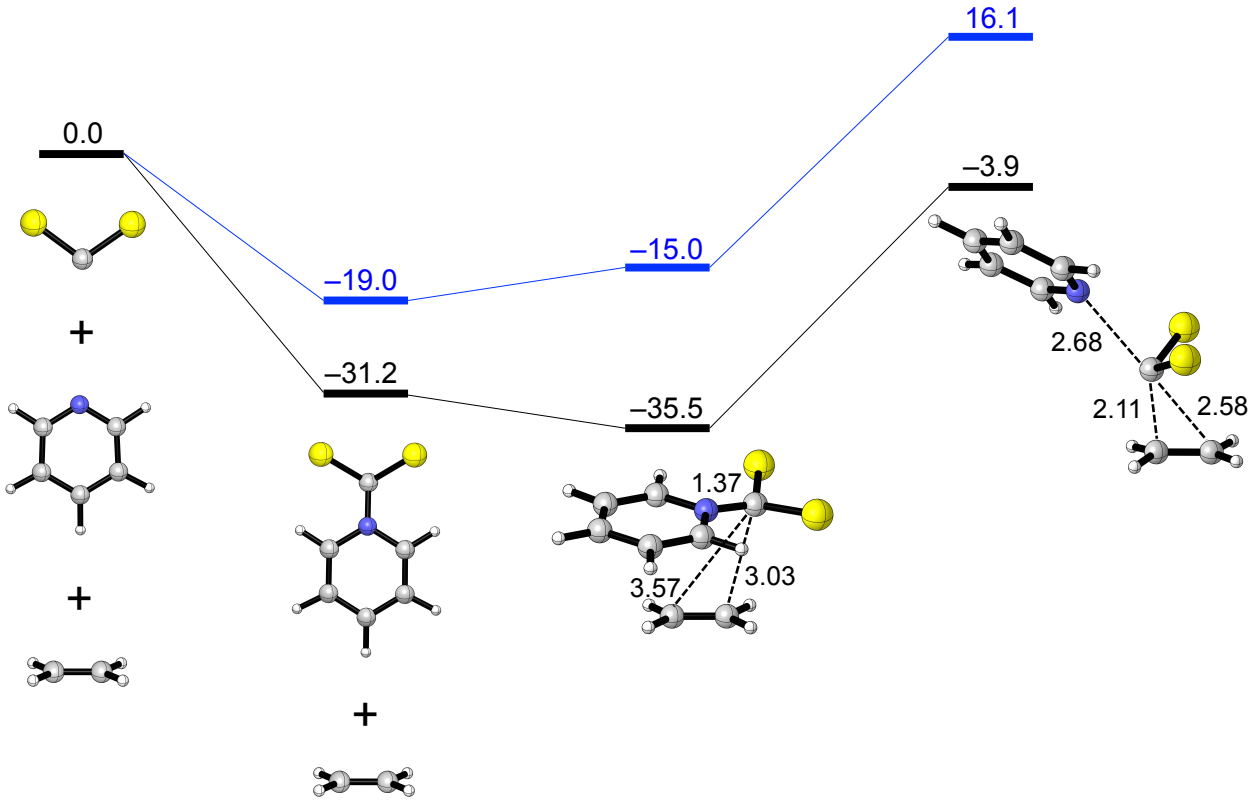


**Figure 2.9.** Stationary points for the formation and addition of $CCl_2$-pyridinium ylide to ethylene. The black line is ΔH and the blue line is ΔG in kcal/mol computed at the M06-2X/6-31+G(d,p) level of theory.

the complex between the pyridinium ylide and ethlyene is unstable by 4 kcal/mol in terms of free energy. From the computed values of $\Delta H^{\ddagger}$ and $\Delta G^{\ddagger}$ for isolated $CCl_2$-pyridinium ylide and ethylene in Figure 2.9, $-T\Delta S^{\ddagger}$ is computed to be 7.8 kcal/mol. These results prove our hypothesis that the $\Delta H^{\ddagger}$ of carbene addition to an alkene through an ylide intermediate is larger than direct addition of the carbene and is likely due to the energy required to break an additional bond, here the C–N bond, in the transition state. In addition, we propose that the entropic penalty of this route is lower than addition of a free carbene due to the vibrational entropy gained in the transition state from the same breaking bond and from increased translational and rotational

freedom of pyridine. While this proof of concept is helpful, the addition of a carbene to an alkene through a pyridinium ylide intermediate is unlikely to play an important role due to the low concentration of pyridine reported in the experiments.

**Carbene-diazirine ylide formation.**

Ylides between singlet carbenes and their diazirine precursors have been observed spectroscopically[23] and so carbene addition to an alkene can theoretically proceed through a carbene-diazirine ylide intermediate. As a starting point, we computed the thermodynamics of carbene-diazirine ylide formation for carbenes **1a–f** at the B97D/6-31+G(d,p) level of theory, shown in Figure 2.10. Carbenes **1a–e** form diazirine ylides **7a–e** with ΔG ranging from -27 to -8 kcal/mol relative to free carbene and corresponding diazirine, while dimethoxycarbene-diazirine ylide decomposes directly to azine **7f**. Computed transition structures for the addition of carbenes **1a–c** to chloroacrylonitrile **2d** through diazirine ylides **7a–c** are shown in Figure 2.11. It is apparent that $\Delta H^{\ddagger}$ decreases from **8a** > **8b** > **8c**, which is opposite of the trend observed in the free carbenes **1a–c** in Table 2.1. Actually, this trend is not surprising when looking at the stabilization of corresponding diazirine ylides **7a–c**. Under the experimental conditions of these carbene cycloadditions, the concentration of alkene is presumably much larger than diazirine precursor immediately after laser flash photolysis and so ylide formation is not likely.

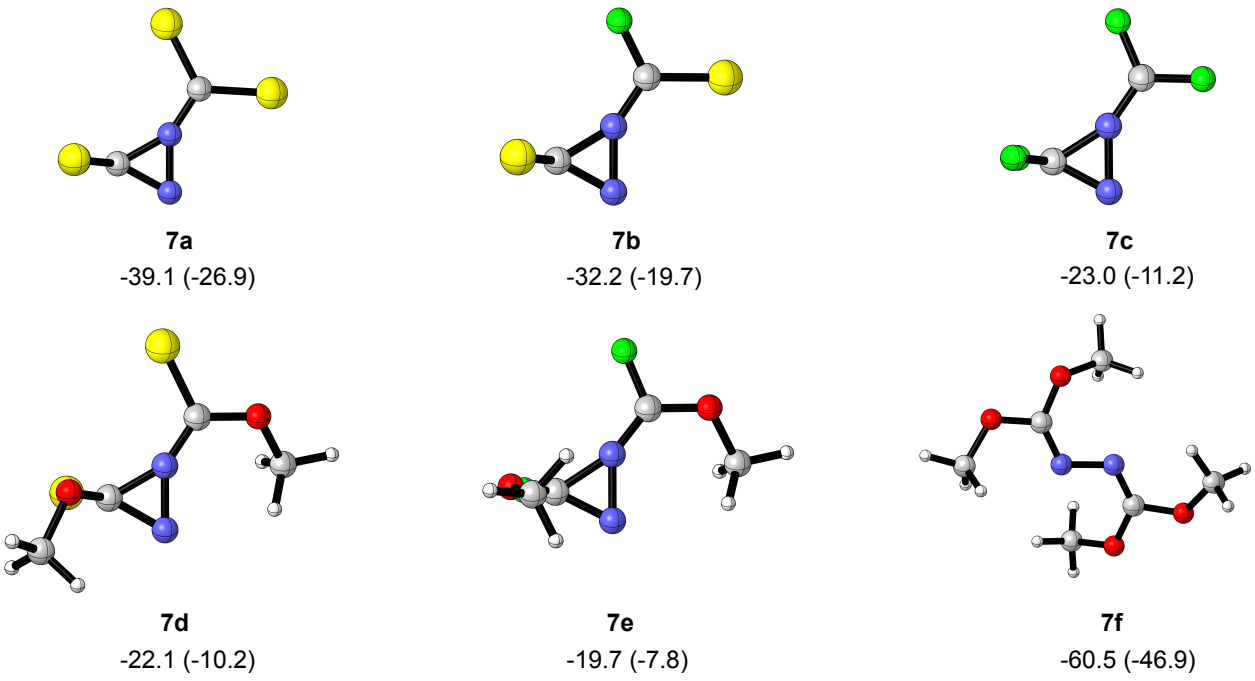


**Figure 2.10.** Optimized structures of diazirine ylides formed with carbenes **1a–f**. Values of ΔH˚ (ΔG˚) in kcal/mol are at the B97D/6-31+G(d,p) level of theory.

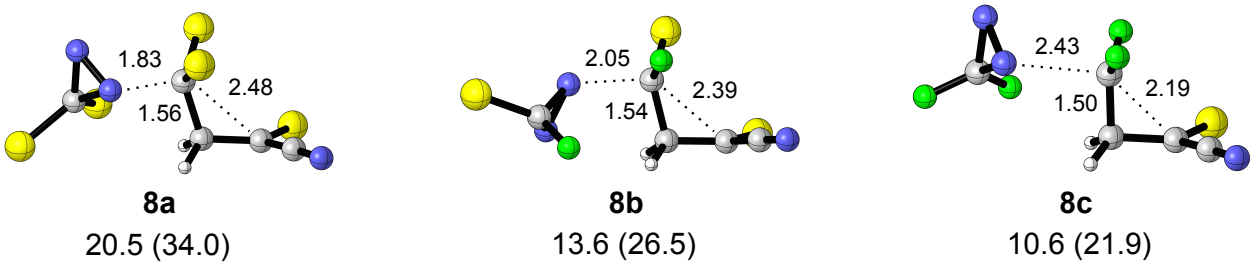


**Figure 2.11.** Computed transition structures of **1a–c** additions to **2d** coupled to diazirine ylide decomposition. Values of $\Delta H^{\ddagger}$ ($\Delta G^{\ddagger}$) in kcal/mol are relative to separated diazirine ylides **7a–c** and **2d** at the B97D/6-31+G(d,p) level of theory. Distances are in Å.

## Conclusions

A computational investigation of carbene cycloadditions to alkenes has been presented in order to address the failure of theory to reproduce experimental activation parameters. Theoretical calculations consistently overestimate the entropic penalties associated with carbene

cycloadditions. Various mechanisms of formal carbene addition to alkenes including the formation of carbene-alkene precursor complexes, carbene-pyridinium ylides, and carbene-diazirine ylides were proposed and tested with electronic structure theory calculations. Cycloadditions from carbene-pyridine and carbene-diazirine ylides result in higher enthalpic barriers and lower entropic barriers relative to cycloaddition of an isolated carbene. However, the resulting values of $\Delta H^{\ddagger}$ are high and decrease with increasing stability of a carbene, providing convincing evidence in opposition to this mechanism. In addition, the concentrations of pyridine and diazirine precursors as well as their carbene ylides are relatively low. It is probable that the inclusion of explicit solvation in computational studies of these systems is necessary in order to gain a complete understanding of experimental results.

## References


1. Bourissou, D.; Guerret, O.; Gabbaï, F. P.; Bertrand, G. *Chem. Rev.* **2000**, *100*, 39–92.
2. Zhang, M.; Moss, R. A.; Thompson, J.; Krogh–Jespersen, K. *J. Org. Chem.* **2012**, *77*, 843–850.
3. Skell, P. S.; Cholod, M. S. *J. Am. Chem. Soc.* **1969**, *91*, 7131–7137.
4. Giese, B.; Meister, J. *Angew. Chem. Int. Ed.* **1978**, *17*, 595–596.
5. Giese, B.; Lee, W.-B. *Angew. Chem. Int. Ed.* **1980**, *19*, 835–836.
6. Giese, B.; Lee, W.-B.; Meister, J. *Ann. Chem.* **1980**, 725–735.
7. Houk, K. N.; Rondan, N. G. *J. Am. Chem. Soc.* **1984**, *106*, 4293–4294.
8. Moss, R. A.; Lawrynowicz, W.; Turro, N. J.; Gould, I. R.; Cha, Y. *J. Am. Chem. Soc.* **1986**, *108*, 7028–7032.
9. Moss, R. A.; Wang, L.; Zhang, M.; Skalit, C.; Krogh–Jespersen, K. *J. Am. Chem. Soc.* **2008**, *130*, 5634–5635.
10. Mammen, M.; Shakhnovich, E. I.; Deutch, J. M.; Whitesides, G. M. *J. Org. Chem.* **1998**, *63*, 3821–3830.
11. Cooper, J.; Ziegler, T. *Inorg. Chem.* **2002**, *41*, 6614–6622.

12. Steinberg, I. Z.; Scheraga, H. A. *J. Biol. Chem.* **1963**, *238*, 172–181.

13. Moss, R. A.; Wang, L.; Krogh-Jespersen, K. *Tetrahedron Lett.* **2014**, *55*, 6016–6018.

14. Hoffmann, R. W.; Lilienblum, W.; Dittrich, B. *Chem. Ber.* **1974**, *107*, 3395–3407.

15. Giese, B.; Lee, W.-B. *Chem. Ber.* **1981**, *114*, 3306–3312.

16. Giese, B.; Lee, W.-B; Neumann, C. *Angew. Chem. Int. Ed.* **1982**, *4*, 310.

17. Yang, N. C.; Marolewski, T. A. *J. Am. Chem. Soc.* **1968**, *90*, 5644–5646.

18. Zutancic, J. J.; Grasse, P. B.; Schuster, G. B. *J. Am. Chem. Soc.* **1981**, *103*, 2423–2425.

19. Houk, K. N.; Rondan, N. G.; Mareda, J. *Tetrahedron* **1985**, *41*, 1555–1563.

20. Blake, J. F.; Wierschke, S. G.; Jorgensen, W. L. *J. Am. Chem. Soc.* **1989**, *111*, 1919–1920.

21. Moss, R. A. *J. Phys. Org. Chem.* **2011**, *24*, 866–875.

22. Jackson, J. E.; Soundararajan, N.; Platz, M. S.; Liu, M. T. H. *J. Am. Chem. Soc.* **1988**, *110*, 5595–5596.

23. Bonneau, R.; Liu, M. T. H. *J. Phys. Chem. A* **2000**, *104*, 4115–4120.

24. Zhao, Y.; Truhlar, D. G. *Theor. Chem. Account* **2008**, *120*, 215–241.

25. Frisch, M. J. et al. (see complete reference in the Supporting Information). Gaussian 09, revision A.1; Gaussian Inc.: Wallingford, CT, 2009.

26. Zhao, Y.; Truhlar, D. G. *Phys. Chem. Chem. Phys.* **2008**, *10*, 2813–2818.

27. Ribeiro, R. F.; Marenich, A. V.; Cramer, C. J.; Truhlar, D. G. *J. Phys. Chem. B.* **2011**, *115*, 14556–14562.

28. Fukui, K. *J. Phys. Chem.* **1970**, *74*, 4161–4163.

29. Deng, L; Ziegler, T. *Int. J. Quantum Chem.* **1994**, *52*, 731–765.

30. Sader, C. A.; Houk, K. N. *ARKIVOC* **2014** (*iii*), 170–183.

31. Houk, K. N.; Rondan, N. G.; Mareda, J. *J. Am. Chem. Soc.* **1984**, *106*, 4291–4293.

32. Mieusset, J.–L.; Abraham, M.; Brinker, U. H. *J. Am. Chem. Soc.* **2009**, *130*, 14634–14639.

33. Hobza, P. *Acc. Chem. Res.* **2012**, *45*, 663–672.

34. Dieckmann, A.; Houk, K. N. *J. Chem. Theory Comput.* **2012**, *8*, 5064–5071.

35. Briegleb, G.; Czekalla, J.; Hauser, A. *Z. physik. Chem.* (Frankfurt) **1959**, *21*, 99–113.

36. Briegleb, G.; Czekalla, J. *Z. Elektrochem.* **1955**, *59*, 184–202.

37. Borhani, D. W.; Shaw, D. E. *J. Comput.-Aided Mol. Des.* **2012**, *26*, 15–26.

38. Mobley, D. L. *J. Comput.-Aided Mol. Des.* **2012**, *26*, 93–95.

39. Moss, R. A.; Wang, L.; Krogh-Jespersen, K. *J. Org. Chem.* **2013**, *78*, 11040–11044.

40. Moss, R. A.; Tian, J.; Sauers, R. R.; Ess, D. H.; Houk, K. N.; Krogh-Jespersen, K. *J. Am. Chem. Soc.* **2007**, *129*, 5167–5174.

## III. Studying $CCl_2$ + Ethylene and $CF_2$ + Ethylene with Condensed Phase Direct Dynamics Simulations

### Introduction

Classical trajectory simulations have been used to study chemical reaction dynamics for years.[1] They provide important atomic-level information such as reaction pathways and intramolecular vibrational energy redistribution rates. A broadly applicable approach for performing these simulations is Born-Oppenheimer direct dynamics for which the potential energy and its gradient, needed to numerically solve the classical equaitons of motion, are obtained directly from an electronic structure theory. In a direct dynamics simulation, the classical equations of motion are numerically integrated without the need for an analytic potential energy function.[2] The direct dynamics approach for performing a classical trajectory simulation was first implemented, using the CNDO semiempirical method, to study the $^1CH_2$ + $H_2 \rightarrow CH_4$ reaction.[3] The initial *ab initio* direct dynamics trajectory simulation was for the $H^-$ + $CH_4 \rightarrow CH_4 + H^-$ $S_N2$ reaction.[4] *Ab initio* direct dynamics simulations in the gas phase have vastly expanded in scope, with the VENUS/NWChem package specifically being implemented to study post-transition state dynamics for propene ozonolysis,[5] carbocation rearrangements on a bifurcating PES,[6,7] and unimolecular dynamics of the twist-boat intermediate in cyclohexane isomerization[8] to name a few examples.

Condensed phase chemical reactions are subject to a number of complications compared to their gas phase analogs including solvent caging[9] and solvent friction. Benjamin studied the photodissociation of ICN in chloroform and the reaction rates of recombination vs. hydrogen abstraction from chloroform by the CN radical. A major conclusion of his work was that significant steric hindrance and slow solvent reorientation reduced the probability to reach a

reactive configuration that led to hydrogen abstraction from a chloroform molecule in the solvent cage relative to the gas phase. This result is an example of the effect of solvent caging on the dynamics of a chemical reaction and is consistent with a lower reaction rate for abstraction in the condensed phase than in the gas phase.[9] The solvent can influence the rate of a chemical reaction by a static, equilibrium modification of activation energies and other activation parameters. Tuñón et al. have investigated the role of solvent fluctuations on a proton transfer from a water molecule to a hydroxyl anion in liquid water. They observed that the reaction proceeds in 20–30 fs, independent of collisions with an essentially frozen-solvent configuration; however, fluctuations in the electric field of the solvent, which occur on the order of $10^1$–$10^2$ fs, modify the instantaneous barrier felt by the proton.[10] Dynamic effects of the solvent can also effect reaction rates. A prominent theory of the dynamic effect of the solvent on an activated barrier passage is from Kramers. According to Kramers theory, low friction corresponds to a situation in which solvent collisions are negligibly effective in inducing barrier recrossing. With limited dynamical coupling to the solvent, the rate of reaction approaches that predicted by transition state theory. Conversely, high friction increases recrossing events and the effective rate of reaction is diminished.[11] Work by Grote and Hynes has shown that, in extreme cases, solvent friction is capable of changing the reaction path.[12]

The goal of this project was to computationally investigate solvent effects on the dynamics of carbene cycloadditions, specifically $CCl_2$ and $CF_2$ + ethylene shown in Scheme 3.1.

**Scheme 3.1.** Cycloadditions of dichlorocarbene and difluorocarbene with ethylene.

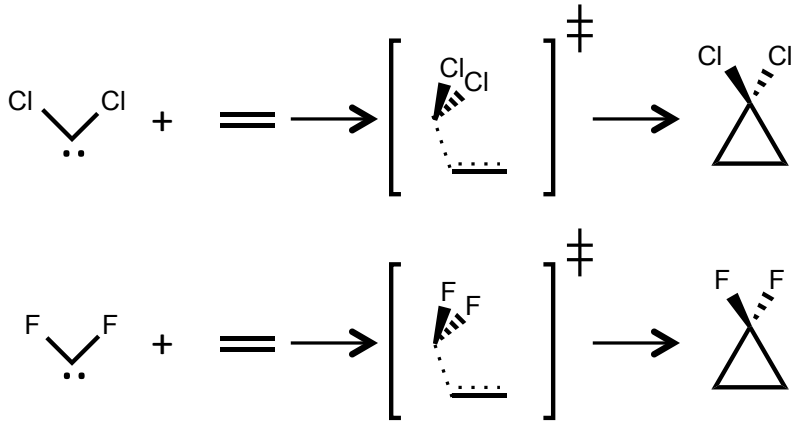


**Computational Methodology**

The gas phase and condensed phase direct dynamics simulations[13] reported here were performed using a model wherein interactions for the reactants are described quantum mechanically and interactions for the solvent and between the reactants and solvent are described with molecular mechanical parameters (QM/MM). A classical trajectory direct dynamics simulation requires identification of an electronic structure calculation method. We chose the B3LYP/6-31G(d) level of theory in order to directly compare our results to previous dynamics studies of these cycloadditions[14] and also to maintain computational efficiency. Even at this modest level of theory, each complete gas phase trajectory took ~5 hours and each condensed phase trajectory took ~10 hours of real time using eight CPUs on a parallel supercomputer cluster. For comparison, one condensed phase trajectory at the M06-2X/6-31+G(d,p) level of theory took >30 hours of real time or ~240 CPU hours. The reliability of B3LYP/6-31G(d) was verified by comparison of stationary points on the cycloaddition potential energy surfaces at higher levels of theory, namely B3LYP–D3/def2–QZVP and M06–2X/def2–TZVPP. In order to generate the condensed phase system, randomly oriented solvent molecules were placed around

the reactive solute system. Then, the solvent was equilibrated at 300 K in increments of 500 ps for a total of 4 ns in a 3D periodic 28.7 Å cubic box with the reactive system held constrained at the center of the box. At the end of equilibration the density of pentane was 0.608 g/mL, an error of about 3% of the experimental density of 0.626 g/mL, and the trans:gauche ratio was 85:15. During the equilibration, ten solvent configurations were stored and subsequently used as starting configurations for the trajectory simulations. The OPLS–AA[15] force field was used to define the intramolecular potential for the pentane molecules as well as non–bonded intermolecular solute–solvent and solvent–solvent interactions. The parameters of the OPLS-AA force field are known to accurately reproduce physical properties of a variety of molecules including alkanes. The software package with the classical dynamics program VENUS[16,17] coupled to the NWChem electronic structure program,[18] developed by the Hase group at Texas Tech,[19] was used for the simulations. Currently, the VENUS/NWChem software package does not include electrostatic embedding, in which the electron density of the solute is perturbed by interaction with the solvent. With a nonpolar solvent like pentane, the lack of electrostatic embedding is not considered to be a critical flaw.

The reactions of $CCl_2$ and $CF_2$ with ethylene were explored with 256 gas phase trajectories and 256 trajectories in explicit pentane. The initial coordinates and momenta were selected by transition state normal mode sampling,[20] which generates a set of structures whose coordinates and momenta approximate a quantum mechanical Boltzmann distribution of vibrational levels on the transition state dividing surface at 300 K. In its present implementation, VENUS uses only the gas phase frequencies for the transition state normal mode sampling; therefore, the same initial conditions were generated for both gas and condensed phase simulations. Although this is a potentially troubling deficiency in the method, we have observed that frequencies of stationary

points on the potential energy surfaces of both reactions are nearly identical in the gas phase and in implicit pentane with the SMD model. In fact, the assumption of identical frequencies in a vacuum and in solution is not uncommon in the field of molecular dynamics simulations.[21,22] All of the trajectories began in the transition state region and were run in both forward and reverse directions from the initially selected point. Trajectories were accepted if one segment formed the adduct and the other segment resulted in separated reactants. The trajectories were integrated using a sixth–order symplectic integrator[23] with an integration time step of 0.2 fs. Symplectic integration of the electronic solution enables highly efficient simulations while keeping a rigourous control over physical properties without a systematic energy drift.

**Results and Discussion**

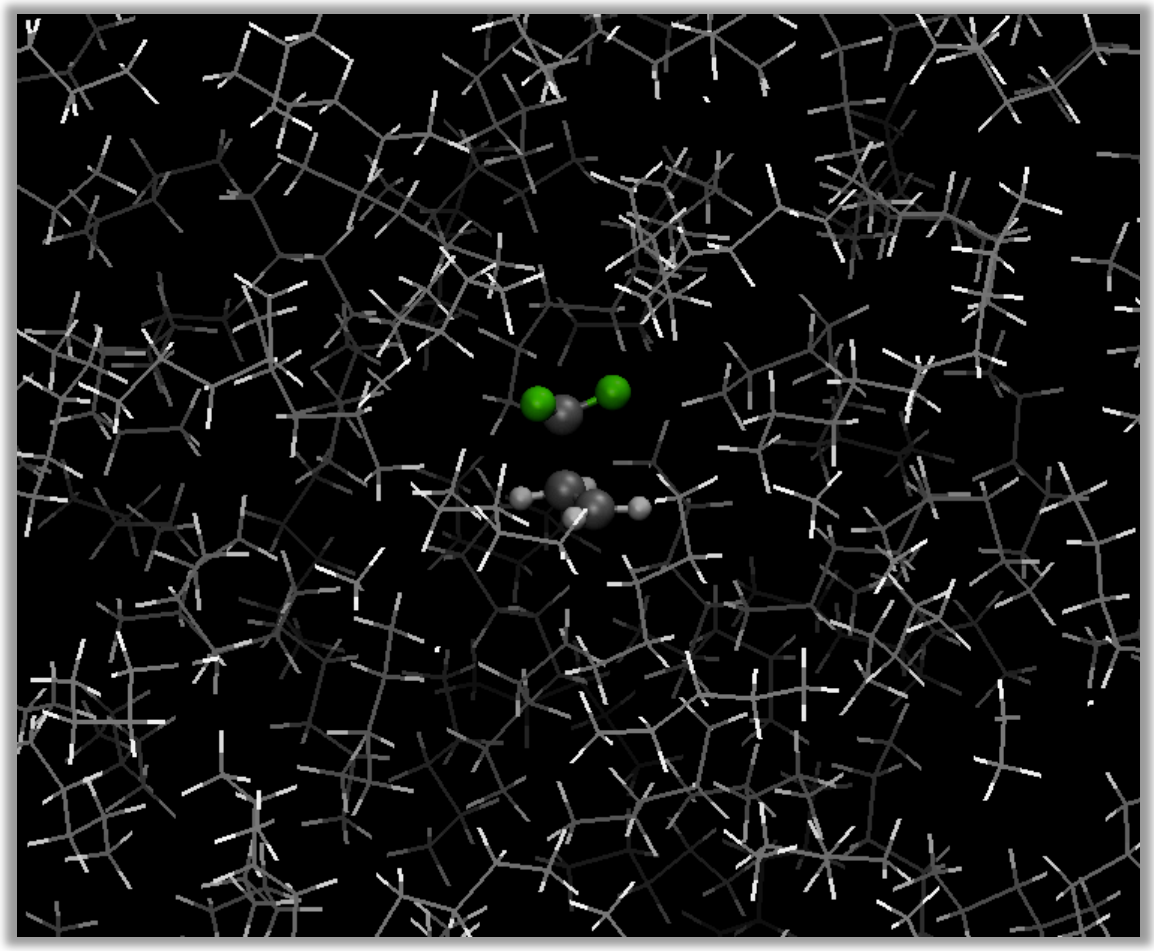

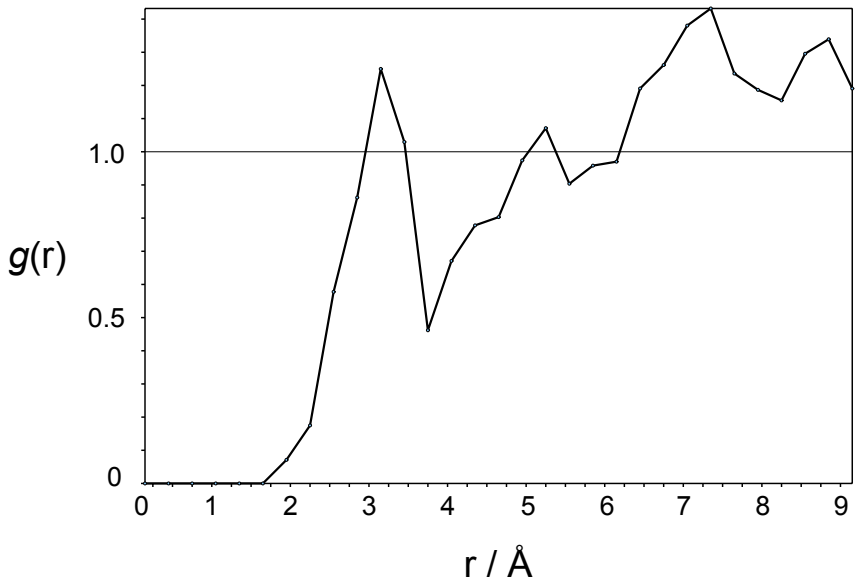


**Figure 3.1.** Solvated transition state of $CF_2$ + ethylene along with a radial distribution function of solvent H – carbene F in the transition state.

Figure 3.1 contains the optimized transition structure of $CF_2$ + ethylene in an equilibrated box of pentane as well as a radial distribution function that shows the distribution of pentane hydrogens around the fluorine substituents of $CF_2$. Beyond the peak at around 3.1 Å corresponding to the hydrogens closest to fluorine, the peaks of the RDF are not clearly resolved because all of the hydrogens on pentane contributed to the calculation and the fluorine substituents are not centered within the solute cavity. Visual inspection of the solute/solvent system indicated that the linear pentane molecules in the first solvation shell are tangential to the spherical solute cavity.

Figures 3.2 and 3.3 show overlays of sampled starting geometries in each of the 225 reactive trajectories for $CCl_2$ + ethylene and 231 reactive trajectories for $CF_2$ + ethylene on the B3LYP/6–31G(d) surface. The distributions of atomic coordinates in the transition states are narrow for each reaction. A previous gas phase study of these reactions[14] shows a distribution of starting geometries for $CCl_2$ + ethylene that is considerably more scattered than that of $CF_2$ +

ethylene, which is attributed to the lower barrier and earlier transition state of the former reaction computed with UB3LYP/6–31G(d) in Gaussian 09. To investigate this apparent discrepancy between previous results and our current results, stationary points with frequency analyses at the UB3LYP/6–31G(d) level of theory were computed with the Gaussian 09 and NWChem software packages. The average differences of the transition state frequencies for $CCl_2$ + ethylene and $CF_2$ + ethylene between the two software packages were 5 $cm^{-1}$ and 7 $cm^{-1}$ with mean absolute deviations of 12 $cm^{-1}$ and 11 $cm^{-1}$, respectively. In addition, the cycloaddition barriers as computed by Gaussian 09 and NWChem were within 1–2 kcal/mol. Based on these results, the Boltzmann distributions in Figures 3.2 and 3.3 are expected to be identical to their counterparts

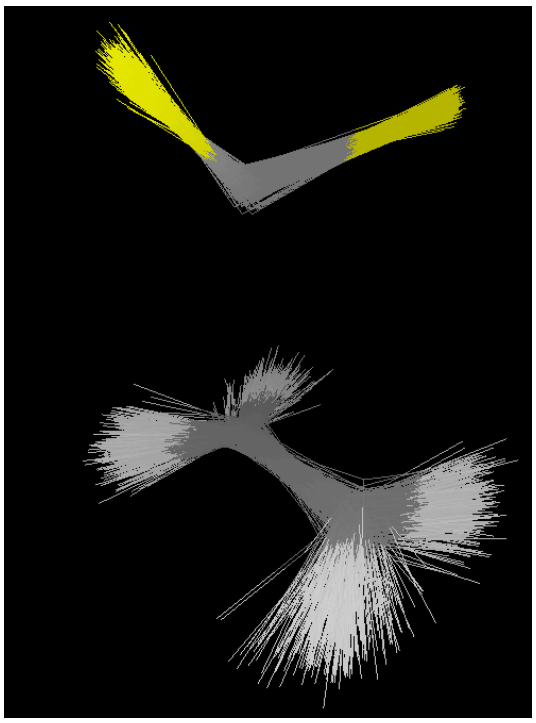

**Figure 3.2.** Overlay of starting geometries of 225 reactive trajectories for the reaction of $CCl_2$ + ethylene.

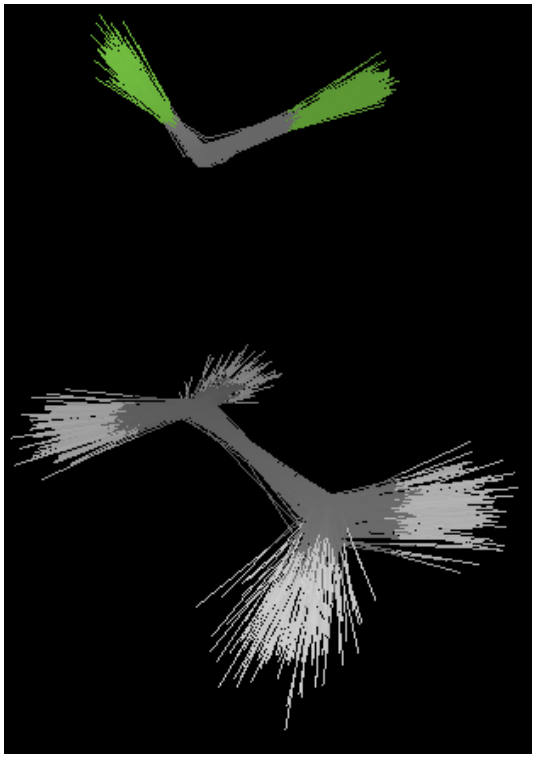

**Figure 3.3.** Overlay of starting geometries of 231 reactive trajectories for the reaction of $CF_2$ + ethylene.

computed with Gaussian 09; therefore, the reason for differences with those in Figure 2 of Ref. 14 is presently inexplicable. It should also be noted that the asynchronicities, which are the differences of the two forming C–C bond lengths in each transition state, averaged over all 256 trajectories were 0.53 ± 0.13 Å for $CCl_2$ + ethylene and 0.65 ± 0.11 Å for $CF_2$ + ethylene, which for all practical purposes are identical to 0.54 ± 0.13 Å and 0.67 ± 0.12 Å found by Xu et al. Figure 3.4 shows snapshots of a representative trajectory for the reaction of $CCl_2$ with ethylene in the condensed phase with the solvent omitted for clarity. The reaction is shown from the formation of a van der Waals complex, defined as a C–C distance of 3.4 Å, 98 fs before the transition state to the formation of a cyclopropane adduct at the point where the second C–C bond length reaches 1.59 Å 54 fs after the transition state. Bond formation is arbitrarily defined here as a C–C distance less than 3.0 bohr or 1.59 Å to directly compare gas phase results with Lai et al.; however, previous values of 1.6 Å and 2.0 Å have also been used.[3] The transition state

structure represents t = 0 and is shown in the sixth panel of Figure 3.3. The cycloaddition is asynchronous with the complete formation of one C–C bond before the other, in accord with Woodward–Hoffmann orbital symmetry rules as well as past evidence from experiments and ab initio calculations. Although this reaction is asynchronous, it is dynamically concerted in the sense that the time gap between bond formation is less than the period of one C–C bond vibration. The trajectory depicted in Figure 3.4 has a time gap of 16 fs. The average time gap between formation of the two bonds is 19 ± 5 fs in the gas phase and 18 ± 4 fs in the condensed phase, implying that the solvent does not change the average dynamical behavior of this cycloaddition. Solvent is likely not to affect ring closure dynamics after formation of the first bond because the second bond is formed much faster than solvent collisions with the reacting system. For a complete representation of solvent effects on the dynamics, the average time gap from VDW complex to product formation was computed. In the case of $CCl_2$ + ethylene in the gas phase, this value is 165 ± 33 fs, while in explicit pentane the value is 143 ± 27 fs. The conclusion is that the difference in dynamics between simulations in the gas phase and in explicit pentane is not statistically significant for these carbene cycloadditions.

Snapshots of a representative trajectory for the reaction of $CF_2$ with ethylene in the condensed phase, again with the solvent omitted for clarity, are shown in Figure 3.5. The VDW complex forms 78 fs before the transition state, the first bond is formed 43 fs after the transition state and the product is formed 21 fs after the first bond is formed. The average time gap for this cycloaddition was determined to be 30 ± 8 fs in the gas phase and 26 ± 6 fs in the condensed phase. Previously obtained dynamics on this reaction in the gas phase showed a time gap of 245 fs at the same level of theory. This large time gap was attributed to the formation of a diradical

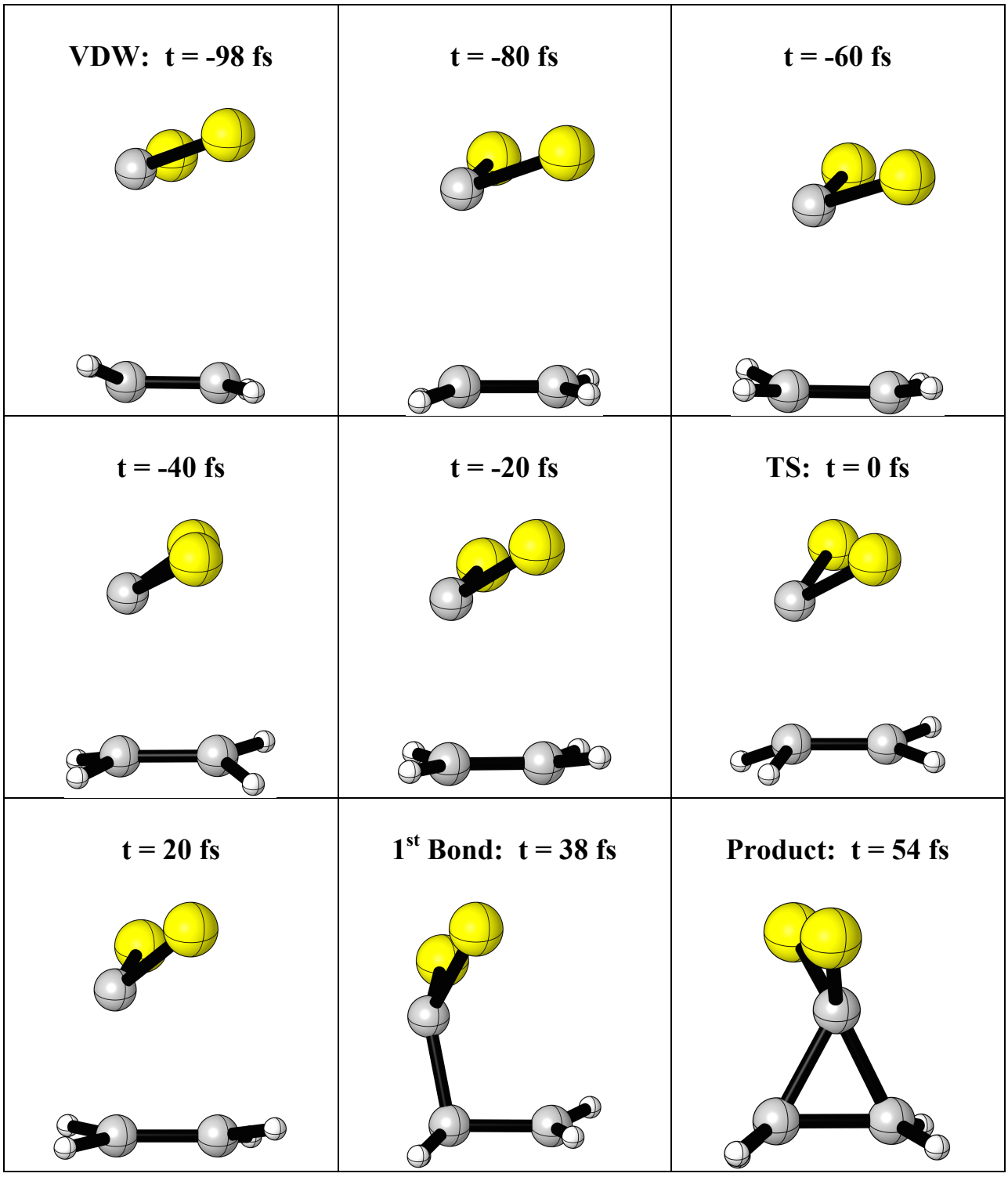


**Figure 3.4.** Snapshots of a representative trajectory for the reaction of $CCl_2$ with ethylene. Frames are snapshots starting from van der Waals complex and ending with product formation.

intermediate with a barrier to inversion of $CF_2$ in order for ring closure to occur.[14] It has long been known that IRCs for dihalocarbene additions involve sequential bond formation,[24–26] and Kraka and Cremer have suggested the presence of intermediates in carbene additions based on their Unified Reaction Valley approach.[27,28] However, we did not locate a diradical intermediate at the UB3LYP/6-31G(d) level of theory using either NWChem or a calculation of the intrinsic reaction coordinate in Gaussian 09. The average time gaps from VDW complex formation to product formation are 169 ± 22 fs in the gas phase and 151 ± 18 fs in the condensed phase, showing that solvent effects do not affect the dynamics of $CF_2$ + ethylene to a statistically significant degree. It is clear from the snapshots in Figures 3.4 and 3.5 that internal C–C bond rotation does not occur in the cycloadditions of $CCl_2$ and $CF_2$ + ethylene. The time gap data are compiled in Table 3.1.

**Table 3.1.** Summary of the time gaps between the formation of the first and second bonds as well as between the formation of a van der Waals complex and the cyclopropane adduct for the cycloadditions of CCl2 and CF2 to ethylene in the gas and condensed phases.

| | Gas phase | | Condensed phase | |
|---|---|---|---|---|
| Carbene | Time gap (fs) | VDW to product (fs) | Time gap (fs) | VDW to product (fs) |
| $CCl_2$ | 19 ± 5 | 165 ± 33 | 18 ± 4 | 143 ± 27 |
| $CF_2$ | 30 ± 8 | 169 ± 22 | 26 ± 6 | 151 ± 18 |

Figures 3.6 and 3.7 show the two forming C–C bond lengths for 50 representative gas phase and condensed phase trajectories for $CCl_2$ + ethylene, respectively. The reactant region is in the upper right corner and the product region is in the lower left corner where both bond lengths are about 1.54 Å. The transition state region is in the grid formed by a $C_1$–$C_2$ bond length of 2.1-2.3 Å and a $C_2$–$C_3$ bond length of 2.6-2.8 Å. The trajectories were manually terminated after a few $C_1$–$C_2$ and $C_2$–$C_3$ bond vibrations in the product basin were observed. Energy redistribution after

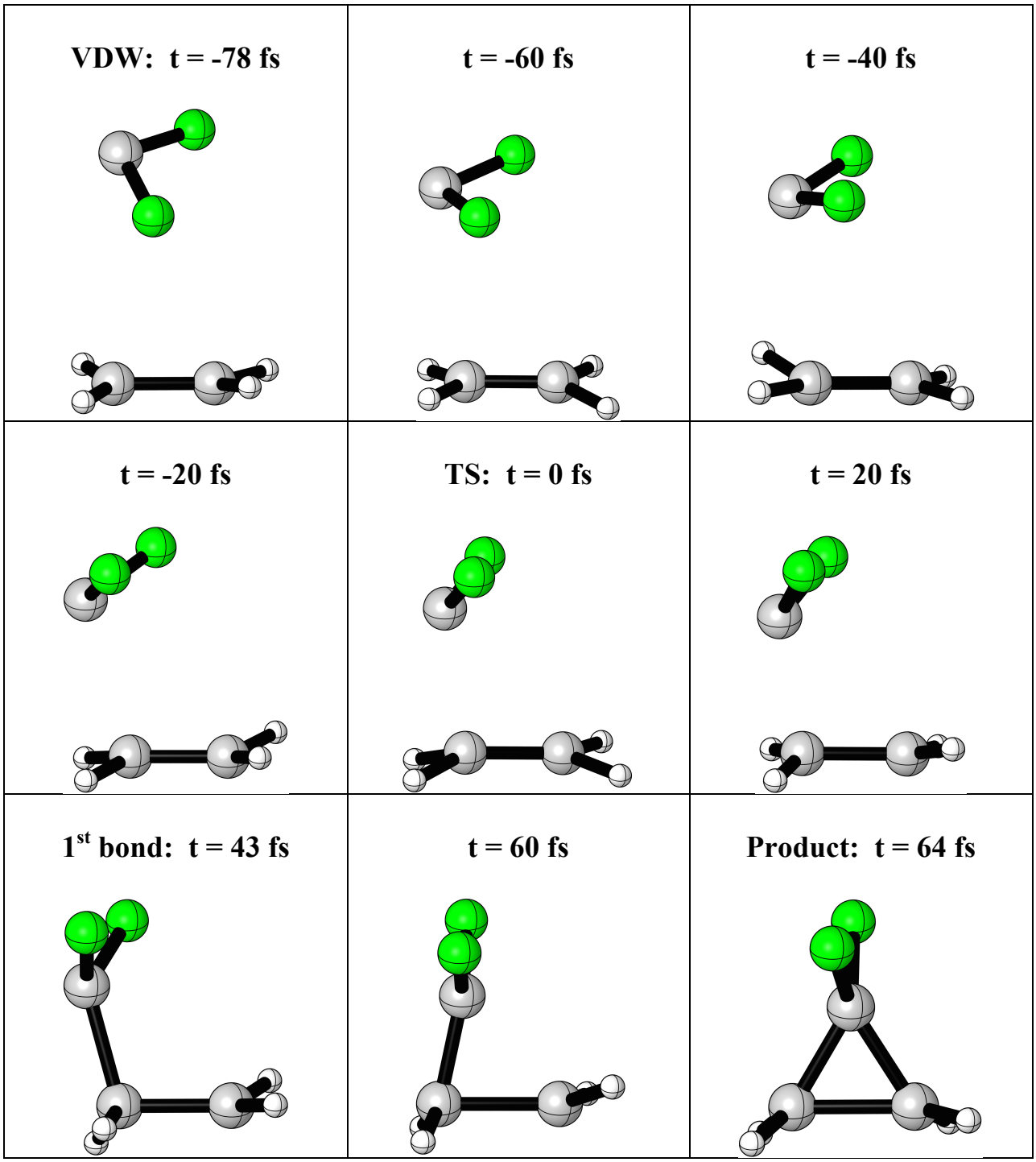


**Figure 3.5.** Snapshots of a representative trajectory for the reaction of $CF_2$ with ethylene. Frames are snapshots starting from van der Waals complex and ending with product formation.

product formation was not the concentration in the present study; however, 30 each of gas phase and condensed phase trajectories were allowed to continue for 5 ps after product formation to

observe the dynamics in the potential energy well of the product. The energies of the products in the gas and condensed phases were not significantly different after 5 ps. Similarly, Glowacki et al. observed small solvent perturbations to the reactive free energy surface in the hydrogen abstraction of cyclohexane by CN, which led to similar post-reaction product energy partitioning in the gas and condensed phase simulations. His study indicated that non-equilibrium energy distributions following solution phase bimolecular reactions may persist for hundreds of picoseconds despite frictional damping.[29] It is known that classical dynamics do not preserve zero-point energy constraints[30] and that bimolecular reactions can occur classically without ZPE in the modes orthogonal to the reaction coordinate as the reactive system passes the transition state.[31,32] For intramolecular vibrational energy redistribution, classical dynamics may allow ZPE to flow from a mode in an unphysical manner and thus enhance the rate of IVR.[33,34] It is assumed that this error, if present in these simulations, is present in both the gas and condensed phases and thus cancels out, leaving the relative comparison of energy redistribution robust. Rebounding back to the transition state or reactant regions was not observed in either the gas phase or the condensed phase simulations. The asynchronicity in bond formation of these reactions is highlighted by the formation of the $C_1$–$C_2$ bond while the $C_2$–$C_3$ bond length remains greater than 2.0 Å. Direct trajectories with minimal oscillations of the first bond prior to ring closure support the small time gaps seen in both phases.

Five representative trajectories of $CF_2$ + ethylene in the gas phase and in the condensed phase are shown in Figures 3.8 and 3.9, respectively. The transition state region is in the grid formed by a $C_1$–$C_2$ bond length of 1.8-2.0 Å and a $C_2$–$C_3$ bond length of 2.4-2.7 Å, illustrating the later and tighter transition state as compared to $CCl_2$ + ethylene. All of the trajectories except 30 gas phase and 30 in explicit pentane were manually terminated about 400 fs after product formation,

with the others continuing for 5 ps after product formation. No rebounding from the product region to the transition state or reactant regions was observed because there is not enough vibrational energy in the $C_2$–$C_3$ bond to reverse the trajectory. These trajectories indicate that most of the vibrational energy in the cyclopropane product is present in the $C_1$–$C_2$ bond, which displays oscillations between 1.3 Å and as great as 2.1 Å.

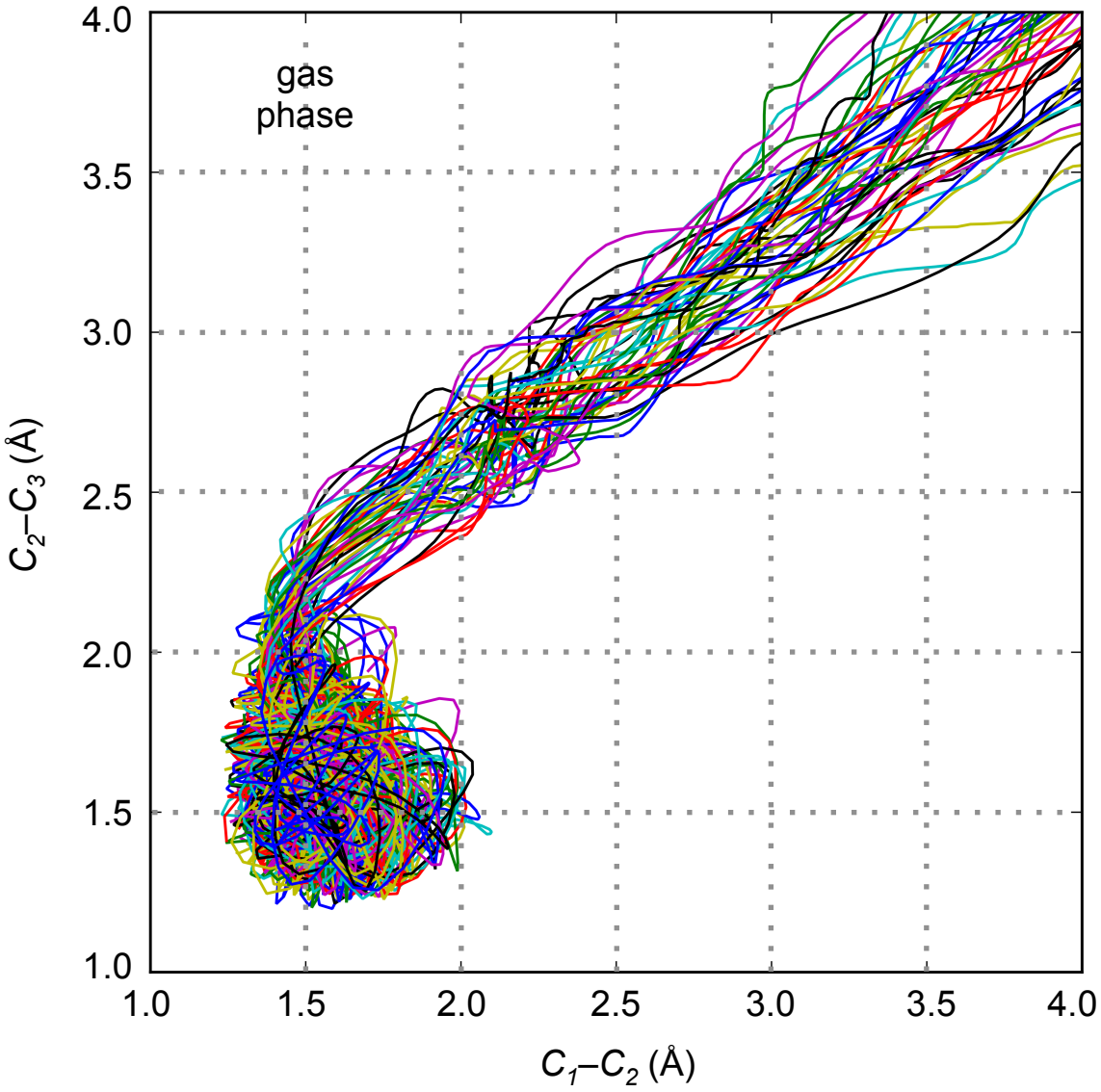


**Figure 3.6.** 50 gas phase trajectories for $CCl_2$ + ethylene projected onto the two forming bonds.

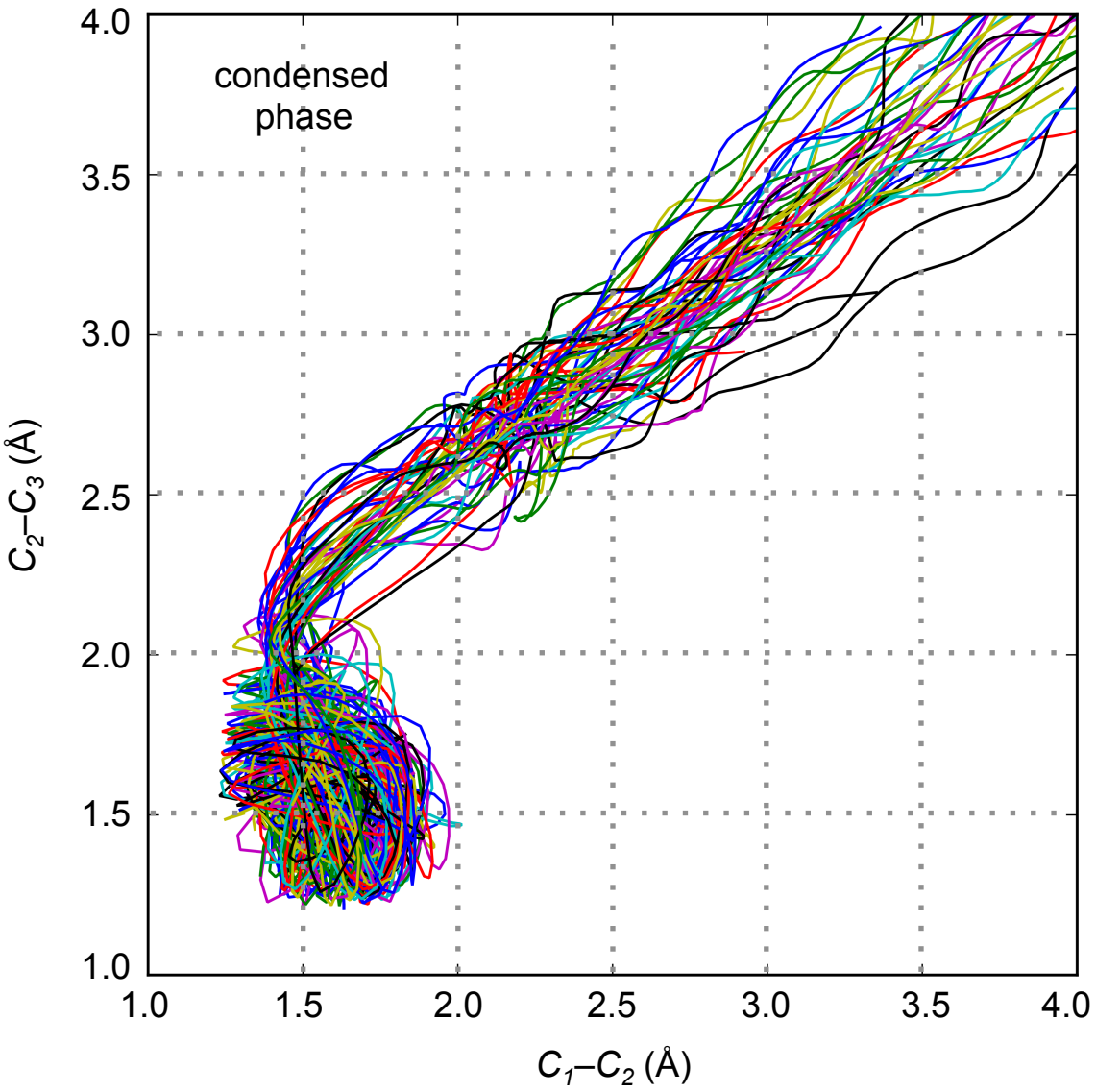


**Figure 3.7.** 50 condensed phase trajectories for $CCl_2$ + ethylene projected onto the two forming bonds.

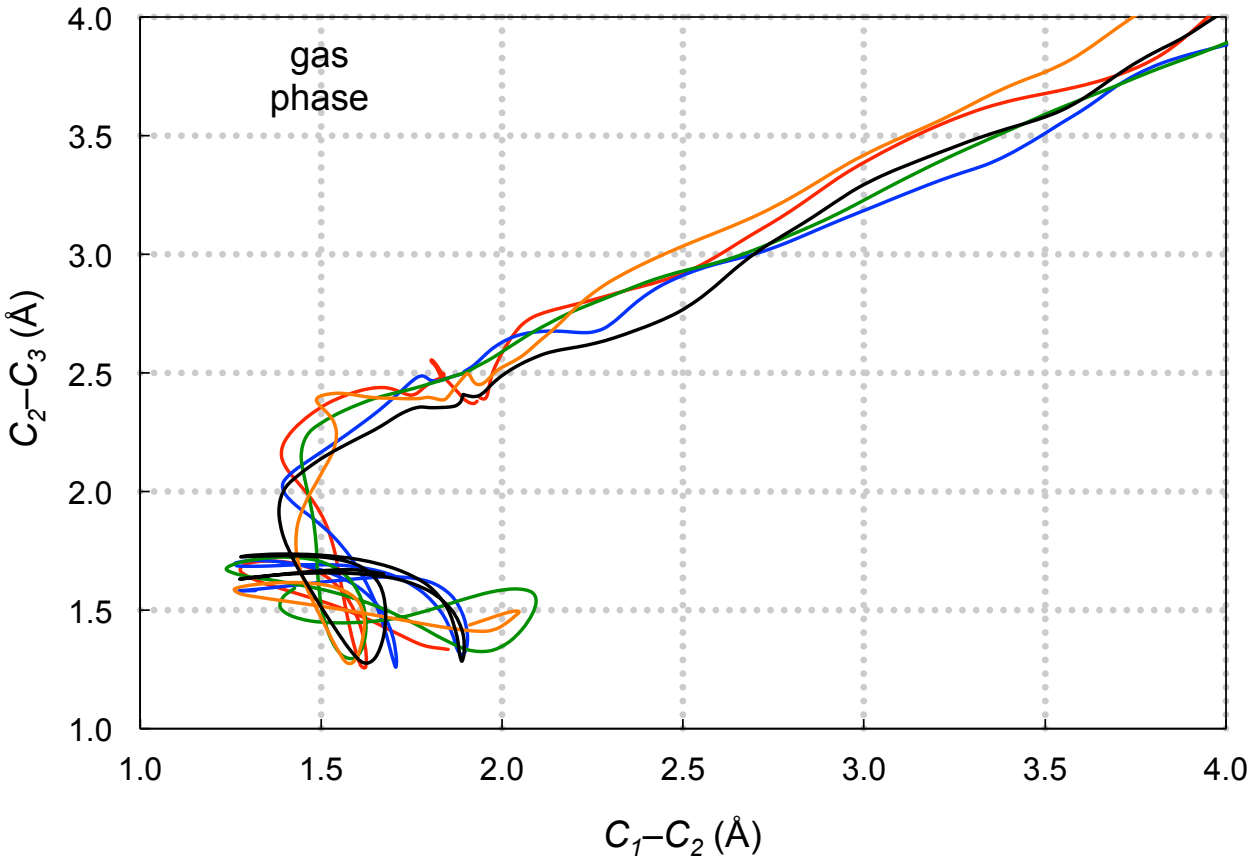


**Figure 3.8.** Five gas phase trajectories for $CF_2$ + ethylene projected onto the two forming bonds.

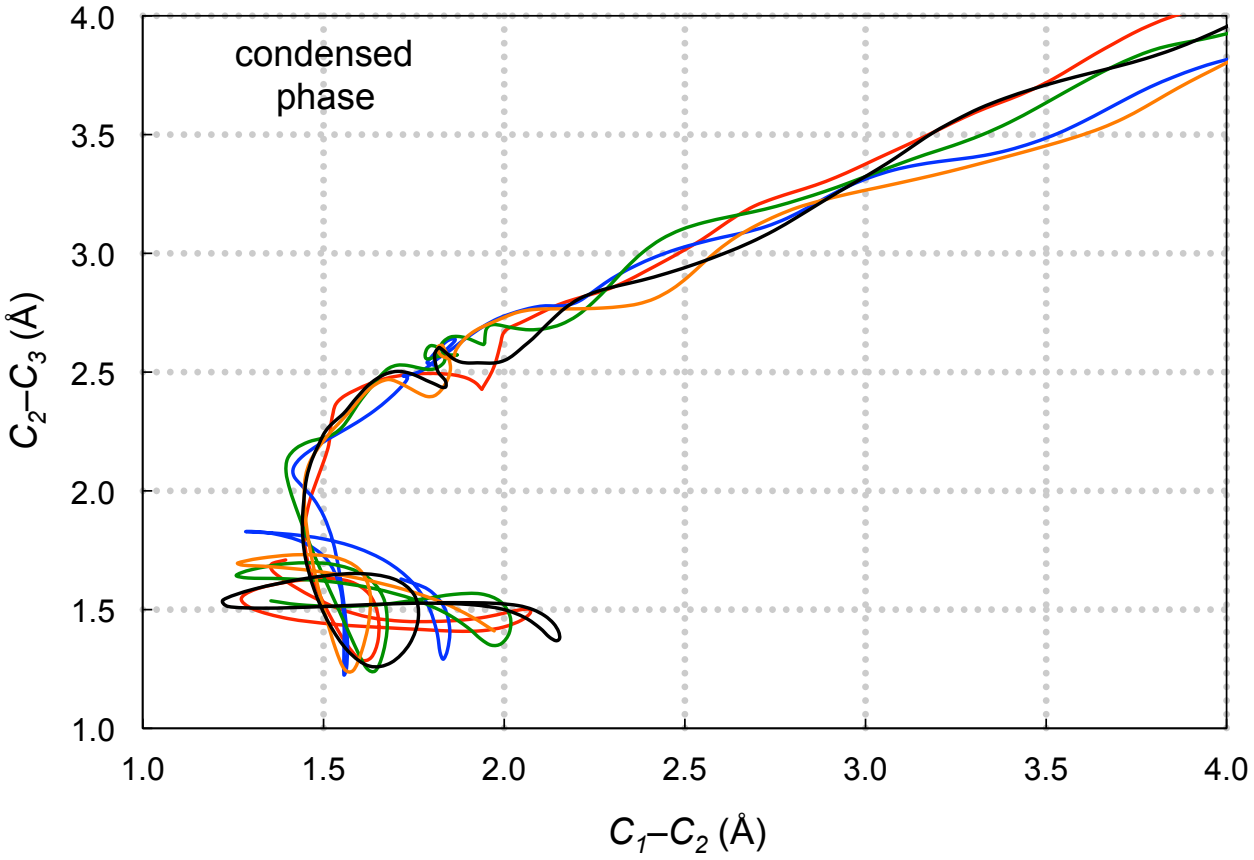


**Figure 3.9.** Five condensed phase trajectories for $CF_2$ + ethylene projected onto the two forming bonds.

## Conclusions

To summarize, these direct dynamics simulations performed in explicit solvent with the VENUS/NWChem software package provide for the first time some insight of carbene cycloadditions to alkenes in an alkane solvent. In the cases of $CCl_2$ + ethylene and $CF_2$ + ethylene observed here, there is no statistical difference in the time of reaction from formation of a van der Waals complex to ring closure to form a cyclopropane product. The known asynchronicity of these reactions was confirmed in the condensed phase simulations and both cycloadditions were shown to be dynamically concerted with the second C–C bond forming <100 fs after the first bond.

## References


1. Bunker, D. L. *J. Chem. Phys.* **1962**, *37*, 393–403.

2. Bolton, K.; Hase, W. L.; Peslherbe, G. H., *Modern Methods for Multidimensional Dynamics Computations in Chemistry*, D. L. Thompson, ed., World Scientific, 1998, p. 143.

3. Wang, I. S. Y.; Karplus, M. *J. Am. Chem. Soc.* **1973**, *95*, 8160–8164.

4. Leforestier, C. *J. Chem. Phys.* **1978**, *68*, 4406–4410.

5. Vayner, G.; Addepalli, S. V.; Song, K.; Hase, W. L. *J. Chem. Phys.* **2006**, *125*, 014317.

6. Siebert, M. R.; Zhang, J.; Addeppalli, S. V.; Tantillo, D. J.; Hase, W. L. *J. Am. Chem. Soc.* **2011**, *133*, 8335–8343.

7. Siebert, M. R.; Manikandan, P.; Sun, R.; Tantillo, D. J. Hase, W. L. *J. Chem. Theory Comput.* **2012**, *8*, 1212–1222.

8. Kakhiani, K.; Lourderaj, U.; Hu, W.; Birney, D. M.; Hase, W. L. *J. Phys. Chem. A* **2009**, *113*, 4570–4580.

9. Benjamin, I. *J. Chem. Phys.* **1995**, *103*, 2459–2471.

10. Tuñón, I.; Martins-Costa, M. T. C.; Millot, C.; Ruiz-López, M. F. *J. Chem. Phys.* **1997**, *106*, 3633–3642.

11. Kramers, H. A. *Physica (The Hague)* **1940**, 7, 284–304.

12. Grote, R. F.; Hynes, J. T. *J. Chem. Phys.* **1981**, 74, 4465–4475.

13. Sun, L.; Hase, W. L. *Rev. Comput. Chem.* **2003**, *19*, 79–146.

14. Xu, L.; Doubleday, C. E.; Houk, K. N. *J. Am. Chem. Soc.* **2011**, *133*, 17848–17854.

15. Jorgensen, W. L.; Maxwell, D. S.; Tirado–Rives, J. *J. Am. Chem. Soc.* **1996**, *118*, 11225–11236.

16. Hase, W. L.; Duchovic, R. J.; Hu, X.; Komornicki, A.; Lim, K. F.; Lu, D.–H., Peslherbe, G. H.; Swamy, K. N.; Vande Linde, S. R.; Varandas, A.; Wang, H.; Wolf, R. J. *QCPE Bull.* **1996**, *16*, 671.

17. Hu, X.; Hase, W. L.; Pirraglia, T. *J. Comput. Chem.* **1991**, *12*, 1014–1024.

18. Valiev, M.; Bylaska, E. J.; Govind, N.; Kowalski, K.; Straatsma, T. P.; Van Dam, H. J. J.; Wang, D.; Nieplocha, J.; Apra, E.; Windus, T. L.; de Jong, W. A. *Comput. Phys. Commun.* **2010**, *181*, 1477–1489.

19. Lourderaj, U.; Sun, R.; Kohale, S. C.; Barnes, G. L.; de Jong, W. A.; Windus, T. L. *Comput. Phys. Commun.* **2014**, *185*, 1074–1080.

20. a) Chapman, S.; Bunker, D. L. *J. Chem. Phys.* **1975**, *62*, 2890–2899. b) Peslherbe, G. H.; Wang,

H.; Hase, W. L. *Adv. Chem. Phys.* **1999**, *105*, 171–201. c) Doubleday, C.; Bolton, K.; Hase, W. L. *J. Phys. Chem. A* **1998**, *102*, 3648–3658.

21. Vallet, V.; Wahlgren, U.; Grenthe, I. *J. Am. Chem. Soc.* **2003**, *125*, 14941–14950.

22. Tomasi, J.; Persico, M. *Chem. Rev.* **1994**, *94*, 2027–2094.

23. Schlier, Ch.; Seiter, A. *J. Phys. Chem. A* **1998**, *102*, 9399–9404.

24. Rondan, N. G.; Houk, K. N.; Moss, R. A. *J. Am. Chem. Soc.* **1980**, *102*, 1770–1776.

25. Houk, K. N.; Rondan, N. G.; Mareda, J. *J. Am. Chem. Soc.* **1984**, *106*, 4291–4293.

26. Bernardi, F.; Bottoni, A.; Canepa, C.; Olivucci, M.; Robb, M. A.; Tonachini, G. *J. Org. Chem.* **1997**, *62*, 2018–2025.

27. Joo, H.; Kraka, E.; Quapp, W.; Cremer, D. *Mol. Phys.* **2007**, *105*, 2697–2717.

28. Kraka, E.; Cremer, D. *Acc. Chem. Res.* **2010**, *43*, 591–601.

29. Glowacki, D. R.; Orr-Ewing, A. J.; Harvey, J. N. *J. Chem. Phys.* **2011**, *134*, 214508.

30. Song, K.; Sun, L.; Hase, W. L. *J. Am. Chem. Soc.* **2001**, *123*, 5753–5756.

31. Miller, W. H.; Hase, W. L.; Darling, C. L. *J. Chem. Phys.* **1989**, *91*, 2863–2868.

32. Swamy, K. N.; Hase, W. L. *J. Phys. Chem.* **1983**, *87*, 4715–4720.

33. Hase, W. L. Buckowski, D. G. *J. Comput. Chem.* **1982**, *3*, 335–343.

34. Lu, D.; Hase, W. L. *J. Chem. Phys.* **1988**, *89*, 6723–6736.